UNIVERSITY OF CALIFORNIA
RIVERSIDE

Development of a Highly Sensitive and Quantitative FRET Based Biosensor to Detect Cell Death Pathways

A Thesis submitted in partial satisfaction
of the requirements for the degree of

Master of Science

in

Bioengineering

by

Chitra Hariharan

September 2017

Thesis Committee:
Dr. Jiayu Liao, Chairperson
Dr. Xiaoping Hu
Dr. William Grover

The Thesis of Chitra Hariharan is approved:

_____

_____

_____

Committee Chairperson

University of California, Riverside

ACKNOWLEDGEMENTS

I would like to express my sincere gratitude to Dr Jiayu Liao for giving me an opportunity to be a part of his lab. I also thank him for trusting me with a completely new project on investigating cell death pathways. My seniors, George Way, Zhehao Xiong and Vipul Madahar taught me the various techniques used in the lab and helped me with valuable inputs throughout my research. I will thank Nicole Duong and Dr Shen for assisting me initially as well as undergraduate students Stephanie Sandoval, Gloria Bartolo and scholar Fatma Zehra for their assistance and continuous encouragement throughout my project. The mathematical model and methodology for enzyme kinetic determination has been adapted from a previous graduate student Yan Liu's work. I am also thankful to her for her valuable inputs. I also received ample guidance for data processing techniques from Dr Jun Li, Associate Professor, UCR Statistics Dept. The statistical error analysis using R has been done by her. I am grateful to Dr Kaustabh Ghosh for his initial review of my work and his feedback. I also thank the Genomics team, particularly Mr. David Carter and Clay Clark for helping with the Victor plate reader for MTT assay and the nanodrop instrument respectively. Lastly, this work is dedicated to my husband (Ganesh) and my parents (Hari and Vasanthi) without whose support and prayers, this work would be impossible.

ABSTRACT OF THE THESIS

Development of a Highly Sensitive and Quantitative FRET Based Biosensor to Detect Cell Death Pathways

by

Chitra Hariharan

Master of Science, Graduate Program in Bioengineering
University of California, Riverside, September 2017
Dr. Jiayu Liao, Chairperson

Cell death is a major process in a biological cell that occurs during development, homeostasis and immune regulation in multicellular organisms. Dysregulation of cell death pathway has been implicated in many diseases. Principle cell death pathways include apoptosis, autophagy, necrosis, mitotic catastrophe etc. Knowledge of cell death pathways and the reason the cell chooses to die one way or the other, are key factors to understand the disease, the way it affects the cellular system and subsequent drug discovery.

This study is focused on developing genetically encoded Förster Resonance Energy Transfer (FRET) based biosensors to identify apoptosis and autophagy pathways *in vitro*. FRET is an energy transfer phenomenon which occurs between two spectrum-overlapping fluorophores that are in close proximity. The design of the sensor is based on enzyme-substrate dynamics and consists of a reporter gene fused between fluorescent proteins.

Additionally, FRET based protease assay has been used to determine the kinetics of Atg4A, an enzyme involved in autophagy. The kinetic parameters km, kcat, kcat /km were derived using real time detection method. To take this forward, the sensor will be transfected in H460 lung cancer cell line to identify the type of death the cell chooses on treatment with sumoylation inhibitors that were previously developed in the lab. MTS assay was conducted to establish the supremacy of sumoylation inhibitors over other commercially available drugs. In conclusion, the biosensor developed in this study is highly sensitive in detecting apoptosis and autophagy and can be used to derive quantitative data using FRET technology. It can be used both *in vitro* and in mammalian cells and can differentiate between apoptosis and autophagy. The results of this study can help to expand biomedical knowledge by illuminating the mechanisms of different cell death pathways. This will pave way for simple and non-invasive ways to modulate cell death pathways for therapeutic intervention in the future.

Table of Contents

LIST OF FIGURES

CHAPTER-1

INTRODUCTION

CELL DEATH

According to the National Committee on Cell Death (NCCD) a cell is considered 'dead' if one of the following conditions are met: a) plasma membrane of the cell has lost its integrity b) the cell including its nucleus has undergone complete fragmentation into discrete bodies and/or c) the fragment have been engulfed by an adjacent cell *in vivo*[2]. The fact that some cells die as part of normal development in order to maintain balance and homeostasis was established more than forty years ago. What forms a subject of intense research currently are the roles that cell death plays, manner in which it is regulated and the underlying mechanisms. Cell growth and death interact with each other to ensure that the number and size of cells are proper and balance is maintained in the organism. Naturally occurring deaths have been described as 'programmed cell death' to differentiate them from pathological cell deaths that are not a part of normal development.

Programmed cell death (PCD) is a striking aspect of vertebrate systems. An important reason why cells die is to get rid of harmful cells which could potentially be harmful to the rest of the organism. For instance, when the cell is infected by a virus, it dies to prevent replication of virus to other cells. When cell dies the natural way, it is mostly not needed by the organism or it has lost its function or it has acquired some mutation. Absence of a regulated cell death mechanism leads to accumulation of genetic mutations and creates an environment of genetic instability. This creates a situation of cells growing out of control

and forming tumors leading to cancer. Among cells of the immune system, positive and negative selection takes place wherein cells that attack the organism's own cells are eliminated. During early embryo formation, cell death helps in digit formation, the lack of which leads to a condition called "syndactyly" that is characterized by webbed fingers and toes[9] (fig1).

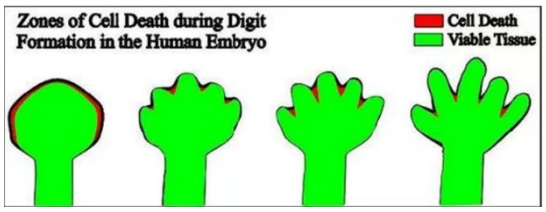

Figure 1. Development of limbs in vertebrates by apoptosis of unwanted cells to form digits.

In many cases, such as the vertebrate nervous system, neurons are generated in excess but only those that are able to form functional synaptic connections survive, rest die. In addition to the occurrence of neuronal cell death during normal development due to failure to establish synaptic connections or withdrawal of trophic support, neurons can also die due to toxic insults such as free-radical generation or protein aggregates. This way of cell death could result in several neurodegenerative diseases such as Alzheimer's disease, stroke, seizures, Parkinson's disease etc[28]. Death of neurons triggered by absence of extrinsic factors needed for survival is studied in context of nerve cell development and presence of extrinsic factors causing cell death is studied in context of neurological disorders (fig 2).

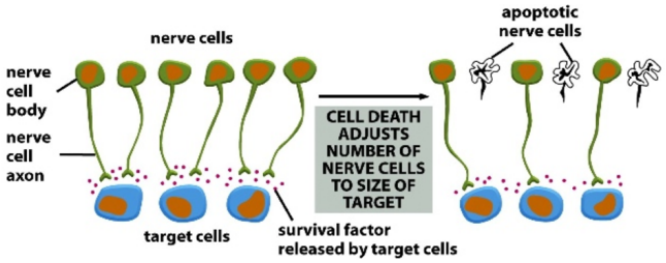

Figure 2. Apoptosis in nerve cells and death of neurons that fail to form synaptic connections.

In the cardiovascular system, the adult cardiomyocyte has limited ability to proliferate. Cardiomyocyte apoptosis plays a key role in formation of heart especially the formation of septa between cardiac chambers and valves. If this process is not regulated, it can result in congenital heart disease. During transition from fetal to adult heart circulation, myocyte apoptosis happens in the interventricular septum and right ventricular wall. The conducting tissue also undergoes apoptosis. Different rates of apoptosis have also been implicated in human heart failure with rates up to 35.5%. Cardiomyocyte apoptosis has been viewed as the mechanism of gradual deterioration in cardiac function. Aging has been associated with myocardial cell loss. Ischemia, deprivation of oxygen/glucose and serum withdrawal are some triggers that can induce apoptosis or necrosis which leads to myocardial infarction[30]. The eye serves as a versatile system to understand how cell death should be properly regulated in-order to help it function the way it is supposed to. During the formation of the eye, as the optic sulcus extends to form the optic vesicle, neural crest derived mesenchymal cells that are present between the optic vesicle and ectoderm undergo apoptotic cell death so that optic vesicle comes in contact with the ectoderm as shown in (fig 3). Some studies have revealed that in absence of apoptosis, the mesenchymal cells continue to proliferate

leading to a condition called anophthalmia[29]. During morphogenesis of the lens of the eye, fibroblast growth factor helps in survival and differentiation of lens fiber cells. Deprivation of the growth factor leads to apoptosis of the cells and an abnormal lens structure. Thus suppression of apoptosis in cells of the lens lineage is an essential step during development. In the adult, when inflammatory cells enter the eye, pro-apoptotic agents such as Fas ligand and transforming growth factor-β express themselves to kill these cells, preventing inflammation and loss of vision[29].

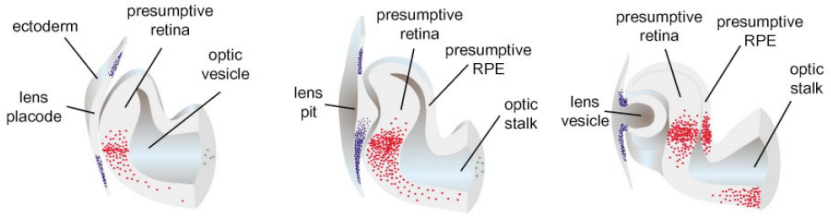

Figure 3. Death of cells occur in ventral aspect of presumptive retina and ventral and anterior part of optic vesicle (shown by red and green dots).

Degradation of cytoplasmic organelles and constituents within the lysosomes by a process known as autophagy has been observed at birth. When the trans-placental nutrient supply is cut off, neonates experience starvation until nutrients are restored through milk. Levels of autophagy which remain low during embryogenesis are found to be upregulated in tissues immediately after birth for several hours before returning to normal level. This process is essential for homeostasis and has been demonstrated experimentally in mice[31]. While some studies have shown that autophagy acts as a suppressant for cancer progression, there are others that show that autophagy helps in cancer cell metastasis. Activity of autophagy has been seen to decrease in cancer cells. It is most likely that increased protein degradation during autophagy diminishes protein available to stimulate

cells that divide uncontrollably. Autophagy might prevent initiation of tumor by getting rid of organelles such as mitochondria and lysosomes that harbor reactive oxygen species (ROS). This way, it minimizes risk of mutations and genetic instability. Enhancement of tumors were seen in several mice species with deficient Atg6 implying that Atg6 has a tumor suppressive function. Atg6 is associated with both apoptosis and autophagy pathways. In addition, mice deficient in Atg4C exhibit increased risk of developing sarcomas along with a reduced ability to activate autophagy upon starvation.

On the other hand, autophagy also contributes to cancer cell survival. Autophagy gets rid of damaged mitochondria that would otherwise produce ROS and harm cancer cells. It also provides cancer cells with nutrients and oxygen in an environment where they are deprived of it due to poor vascularization. In case of metastasizing cells that detach from extracellular matrix, autophagy is induced to provide them with energy during the process of migration. Autophagy also plays its role in providing cancer cells resistance to chemotherapy and aggressiveness. In cancer cells that are treated with chemotherapeutic agents, autophagy has been detected[32].

Need to identify cell death

It is clear at this stage that both apoptosis and autophagy work to establish homeostasis and regulation. Dysregulation of either would harm this delicate balance and can lead to several pathologies. Often the modalities by which the cells die is key to the outcome of cell death at organismal level. Identification of the pathway the cells take to die has important therapeutic implications. For example, some tumor cells are resistant to apoptosis, but not to necrosis triggers. Designing drugs that can induce one cell death pathway (in this case,

necrosis) as opposed to another(apoptosis) has therapeutic advantages. In case of autophagy, there are still gaps in understanding how the process contributes to pathogenesis. To produce compounds that can influence autophagy and deliver promising candidate drugs to target autophagy, there is a need for a specific and sensitive technology to identify and understand thoroughly the underlying mechanisms.

CELL DEATH PATHWAYS

Different types of cell death are defined based on a) morphological criteria such as apoptotic, necrotic, autophagic and mitotic catastrophe b) based on enzymes involved such as different classes of proteases such as caspases, calpains, cathepsins, transglutaminases and nucleases c) based on functional aspects such as programmed, accidental, physiological or pathological cell death and d) based on if it is immunogenic or non-immunogenic[7].

Apoptosis

The term "apoptosis" (pronounced aepu'tosis) which means in Greek "to fall off " was used for the first time in 1972 to describe a certain form of cell death that occurred as part of normal and controlled part of the organism's growth and development. Distinct morphological characteristics include cell shrinkage and condensation, collapse of cytoskeleton, disassembling of nuclear envelope and fragmentation of nuclear DNA. The cell surface is altered and the cell displays properties that causes it to be phagocytized by a neighboring cell or a macrophage[2] (fig4).

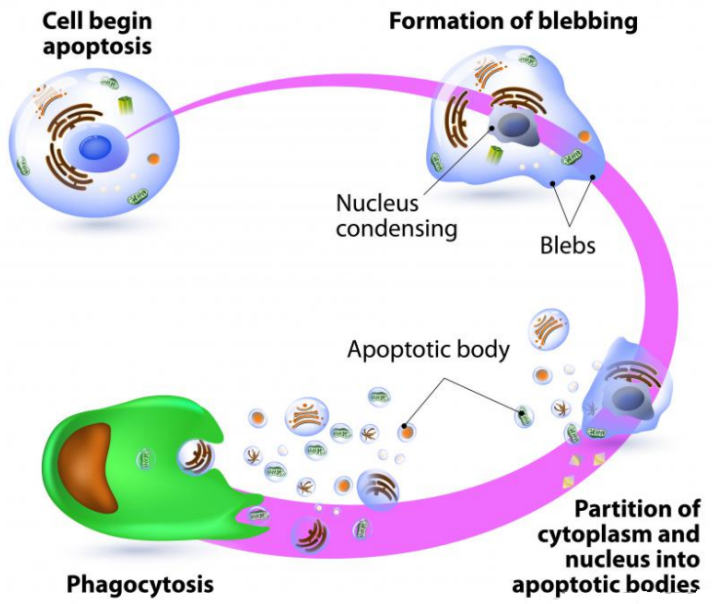

Figure 4. The morphological characteristics of apoptosis. When apoptosis is initiated, the nucleus condenses, blebs are formed. This is followed by partition of cytoplasm and fragmentation of cell into apoptotic bodies and phagocytosis[10]

The most notable part of apoptosis was the absence of inflammation around the dying cell. Apoptosis is also described as "Type-1" or "programmed" cell death because of its tightly regulated mechanism. It is also the primary or default pathway chosen by cells to die when exposed to trigger signals such as DNA damage, viral infection, maturation signals during development, hypoxia, oxidative stress etc. Initiation of apoptosis can happen by signals from either inside the cell, then the apoptosis triggered is said to be **intrinsic or mitochondrial apoptosis** or from outside the cell called the **extrinsic apoptosis**. Both these pathways converge to a common apoptotic pathway[3]. Two main protein families that are evolutionarily conserved are involved in apoptosis. The Bcl-2 family that control the mitochondrial integrity as well as the cysteine aspartate-specific proteases or caspases which mediate the execution phase.

Intrinsic Pathway

The intrinsic pathway acts through the mitochondria and involves the Bcl-2 family proteins. These proteins play a prominent role in regulation of apoptosis and consists of both pro-apoptotic and anti-apoptotic members that interplay to ensure this regulation. All members of the family share at least one Bcl-2 homology (BH) domain. In homeostatic conditions, anti-apoptotic members such as Bcl-2, Bcl-xL and Mcl-1 keep the outer membrane of the mitochondria intact. Under stressing conditions such as cytotoxic insults and DNA damage, the inhibition of the pro-apoptotic members such as Bax, Bid and Bak is relieved as explained in (fig 5). They migrate to the mitochondria, undergo oligomerization and form a channel at the outer membrane. One mechanism suggests that these proteins form pores in the mitochondrial outer membrane and another mechanism suggests that the inner membrane of the Permeability Transition Pore Complex (PTPC) opens with the help of mitochondrial channel proteins such as Adenine Nucleotide Transporter (ANT) and Voltage Dependent Anion Channel (VDAC). This ultimately enhances the permeability of the outer membrane of the mitochondria leading to a condition known as Mitochondrial Outer Membrane Potential (MOMP). Once MOMP occurs, a large number of proteins are released from the inter membrane space of the mitochondria to the cytosol. These include proteins such as cytochrome c, apoptosis inducing factor, endonuclease G, direct IAP binding protein (DIABLO or SMAC) among many others. Cytochrome c binds to Apoptotic protease activating factor-1 (APAF-1) and this induces the formation of a complex called apoptosome which recruits caspase-9.

Caspase-9 is cleaved in the apoptosome and this inturn activates other molecules of caspase-9 and downstream caspases.

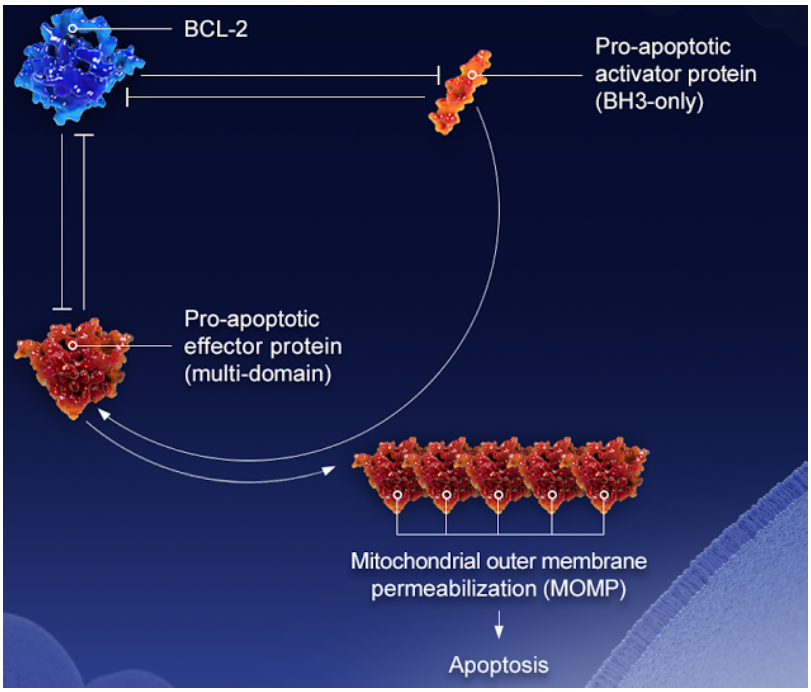

Figure 5. Interplay between anti-apoptotic and pro-apoptotic proteins to initiate and regulate apoptosis[11]

Extrinsic Pathway

Extrinsic apoptosis is triggered by extracellular stress signals which leads to the ligands binding to receptors belonging to the TNFR family such as TNF-receptor1 (TNF-R1), Fas (Apo-1 or CD95), TNF related apoptosis inducing ligand receptor-1 (TRAIL-1), TRAIL-2 and DR6, also otherwise called death receptors. Upon binding of Fas ligand (say for instance), the Fas receptor contains a death domain (DD) in its cytoplasmic region which interacts with the adaptor protein Fas associated death Domain (FADD) and assembly of a multi-protein complex known as Death Initiation Signaling Complex (DISC). Apart from DD, FADD also has death effector domain(DED) and this recruits pro-caspase8 which also

has the DED into the DISC. Pro-caspase8 is then cleaved to active caspase-8 which activates further downstream caspases[5]. Both intrinsic and extrinsic pathways are summarized in the below (fig 6).

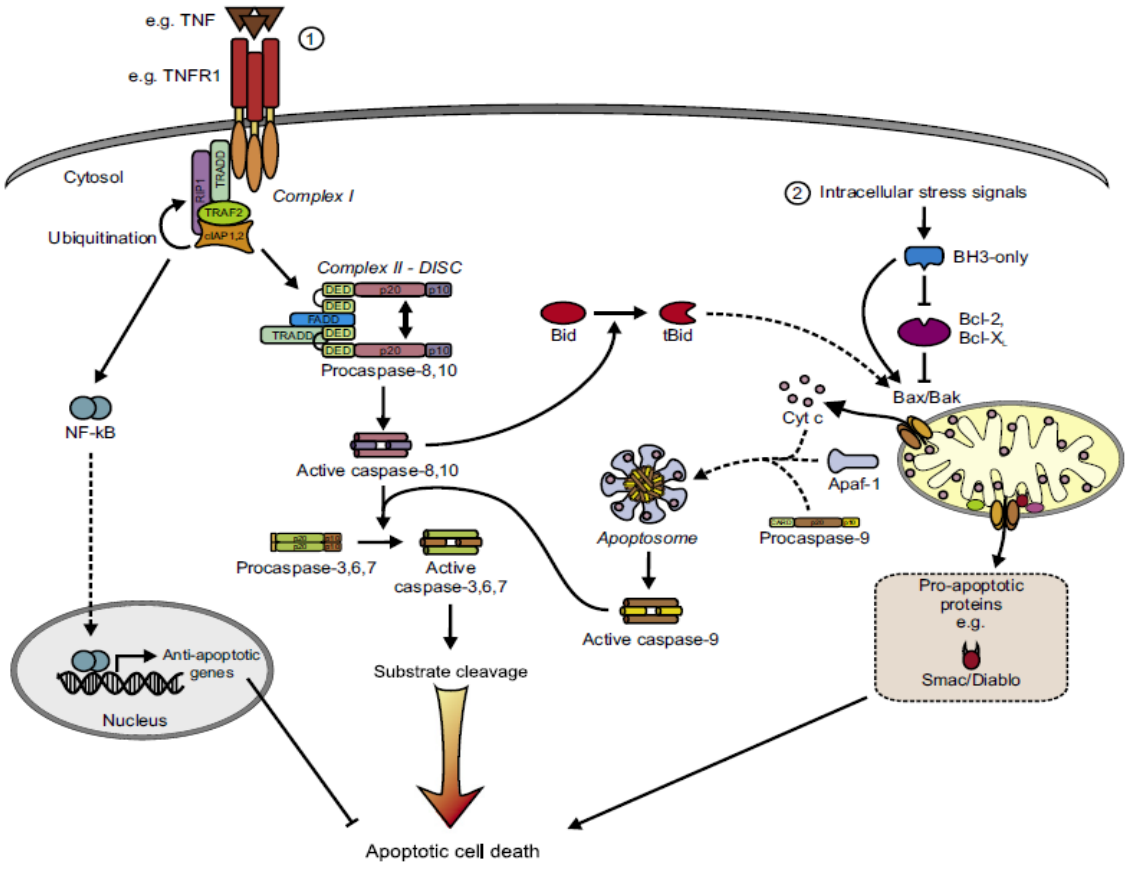

Figure 6. Intrinsic and extrinsic pathways. 1) when TNF ligand binds to the receptor, complex1 and later complex2 is formed which triggers the cascade of caspases leading to apoptosis 2) Stress signals within the cell trigger the Bcl-2 family pro-apoptotic proteins that triggers apoptosis through the mitochondria.

Binding of TNF-α to TNF receptor(TNFR-1) leads to sequential formation of two complexes. Complex-1 consists of TNFR-1, TNF-R associated Death Domain (TRADD), TNF receptor associated factor-2 (TRAF2), Receptor Interacting Protein (RIP1), cellular inhibitor of apoptosis (cIAP-1), cIAP2 and is formed at the plasma membrane. Interaction

between RIP and TRADD can either lead to activation of a transcription factor NF-κB, that leads to transcription of anti-apoptotic genes and cell survival or it can lead to formation of a complex analogous to the DISC that consists of the TRADD, FADD, pro-caspase8 and/or 10. Pro-caspase is then proteolytically cleaved to caspase-8 and/or 10. Caspase-8 can also activate the BH3 domain containing protein Bid which activates the mitochondrial apoptosis suggesting a crosstalk between the intrinsic and extrinsic pathways[7].

Caspases

Caspases are enzymes that belong to a class of cysteine proteases known for its ability to increase the rate of apoptosis and exacerbate disease progression. Interleukin-1ß converting enzyme(ICE)/caspase-1 was the first to be identified as the protease that was responsible for the maturation from pro- Interleukin-1ß to biologically active form. They are unique in the sense that they have an absolute requirement for the presence of Asp at the P1 position of the scissile bond. The caspase gene family has 14 members, of which 11 are known. Caspases belong to two major sub-families: ICD and Ced-3. These are further subdivided based on if they have short or long pro-domains as well as based on substrate specificity[12]. The schematic shown below summarizes the caspase structure (fig 7).

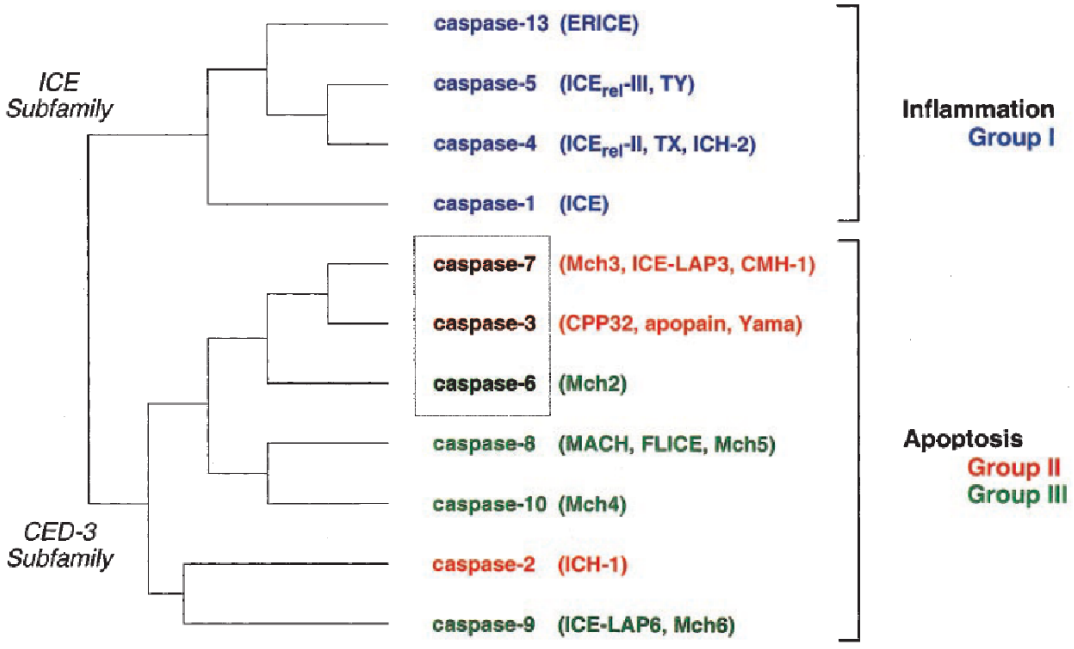

Figure 7. The caspase gene family. Group-1 caspases shown in blue above mainly deal with inflammation and mediate cytokine maturation. Group-2 (in red) and Group-3 (in green) are concerned with apoptosis with group-2 being the effectors and group-3 being the upstream activators[12]

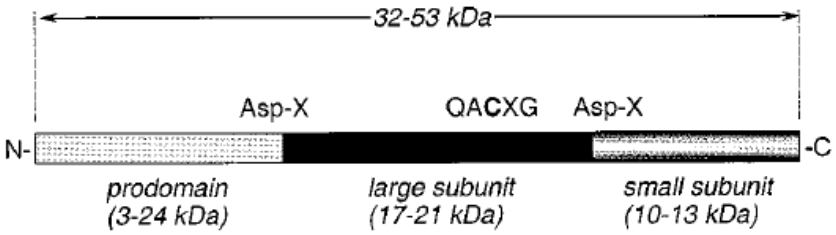

Figure 8. Caspase pro-enzyme organization. The large and small subunit together form the active part of the enzyme and are cleaved from the pro-domain at the Asp(P1)-x(P1') bonds.

Caspases have an N-terminal prodomain and C-terminal catalytic and interaction domain. The caspase catalytic domains include the p-10 and p-20 subunits where the p-20 subunits contain the catalytic residues Cys and His[13] (fig 8)

Proteases act on protein substrate residues around the cleavage site by binding to them. The active site residues in the protease are made of contiguous pockets also called subsites. Each subsite pocket binds to a residue in the substrate sequence also called sequence position. Residues in the substrate sequence are numbered outward from the cleavage site as -P4-P3-P2-P1-P1'-P2'-P3'-P4'- while the subsites in the proteases are correspondingly labelled as -S4-S3-S2-S1-S1'-S2'-S3'-S4'- (fig 9).

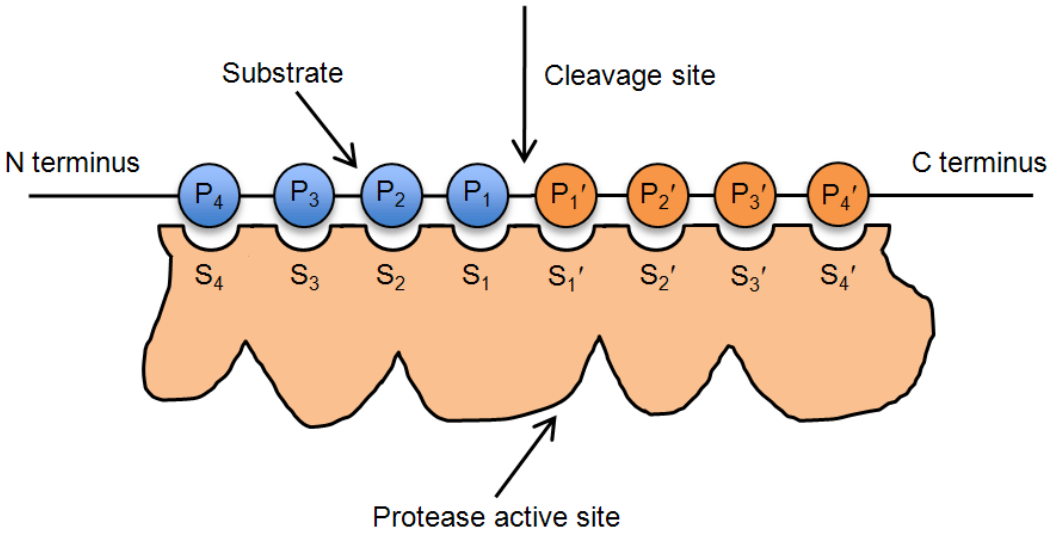

Figure 9. The terminology used for the substrate specificity of protease

Caspases can be divided into three groups based on substrate specificity and they recognize a very short tetrapeptide sequence within substrate polypeptides. These proteases absolutely require Asp in position P1, not much preference in P2, Glu in P3 and different preferences in P4 which puts them in different groups. Group-2 caspases prefer a cleavage motif DEXD which appears in many substrate proteins that are cleaved during cell death thus justifying themselves as effectors of cell death. This is schematically depicted in (fig 10).

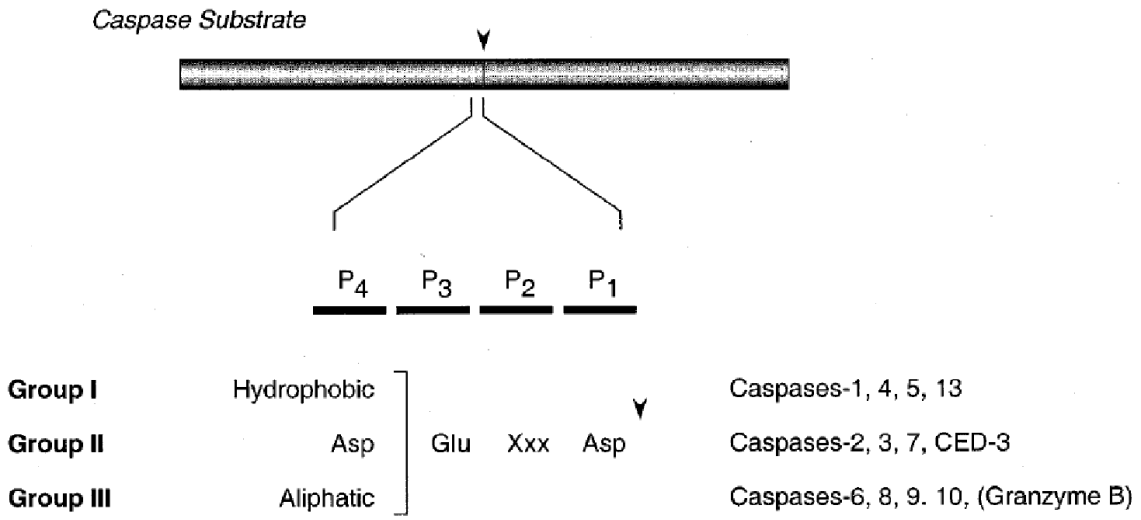

Figure 10. Substrate Specificity of Caspases. Group 1 caspases prefer bulky hydrophobic residues in position P4, group2 require an Asp in P4. Group3 caspases prefer branched chain aliphatic residues in P4[12].

One of the characteristic features of apoptotic cell death includes genomic disassembly and DNA fragmentation. Caspases act by disabling normal DNA repair processes by inactivating at least two proteins that are involved in maintaining genomic integrity – DNA-PK and PARP. Simultaneously an endonuclease caspase activated Dnase (CAD) associated with apoptosis is activated by disabling its cognate inhibitor-ICAD/DFF45. Similar scenarios can be established for most of the substrates that are cleaved by caspases during cell death. Fewer than 200 polypeptides have been estimated to be cleaved by caspases and 70 of these have been identified. The net effect of the cleavage events include 1) disable homeostatic and repair processes 2) halt cell cycle progression 3) inactivate inhibitors of apoptosis 4) mediate structural disassembly and morphological changes and 5) mark the dying cell for engulfment and disposal[12]. To carry out these events, caspases modify their target substrates in any one of the following ways: They either inactivate the

normal function of their substrates such as ICAD, PARP, DNA-PK or activate by removing regulatory domains such as cPLA2, SREBP, PKCs. Caspases can also alter or invert the function of their target substrates. Lastly caspases also play a proteolytic role in cytoskeleton disassembly during apoptosis. Within the target polypeptide, caspases usually cleave within a single site, or multiple sites that are nested or sites that are distal or clustered sites.[12]

Autophagy

Autophagy is an evolutionarily conserved natural mechanism for degradation of cellular components of cytoplasm. It serves as a cell survival mechanism during periods of starving. If there are no nutrients available in the surroundings, the cell is forced to break down a part of its own reserves to survive until situation improves. Although autophagy function as a protective factor for the cells, it also plays a role in cell death. Contradictions have emerged in literature as to whether autophagy is a suicide pathway or cell survival pathway or both. Basal levels of autophagy are required to maintain homeostasis; unregulated degradation of cytoplasm is likely to cause more harm than benefit. It is very important thus that autophagy is tightly regulated and is induced only when required. Autophagy is mostly a pro-survival mechanism that exerts its housekeeping function by ensuring organelle and protein turnover under homeostatic conditions. It could also function by activating type2 autophagic cell death. This would include selected degradation of essential cytoplasmic factors needed for survival. Autophagy is known to exhibit dual role by acting as a balance between cell survival and cell death. Caspases and autophagy are involved in

complementary cell death pathways where autophagy is activated when caspases are inhibited.[15,16,17]

Autophagy, for a long time could only be observed by electron microscopy as molecular dissection of lysosomes was difficult. Yeast was the first and the most ideal organism to study autophagy. Upon induction under stress factors such as starvation, absence of growth factors or low oxygen levels, a double layered membrane composed of lipid bilayers called phagophore or isolation membrane is formed in the cytosol at phagophore assembly sites(PAS). These generally have an average diameter of 700nm initially and seem to evolve from several portions of the cytoplasm[23]. The phagophore expands by adding on sheets of membrane and enclosing cargo that includes damaged organelles and portions of the cytoplasm and finally forms this double layered membrane called autophagosome. The outer membrane of the autophagosome is then fused to the lysosome and its contents are released for degradation. Enzymes in the lysosome namely the lysosomal hydrolases break the contents and the chemical components namely the amino acids are recycled back into the cytoplasm. The membrane proteins that were used to make the autophagosome are also sent back for reuse[16] (fig 11).

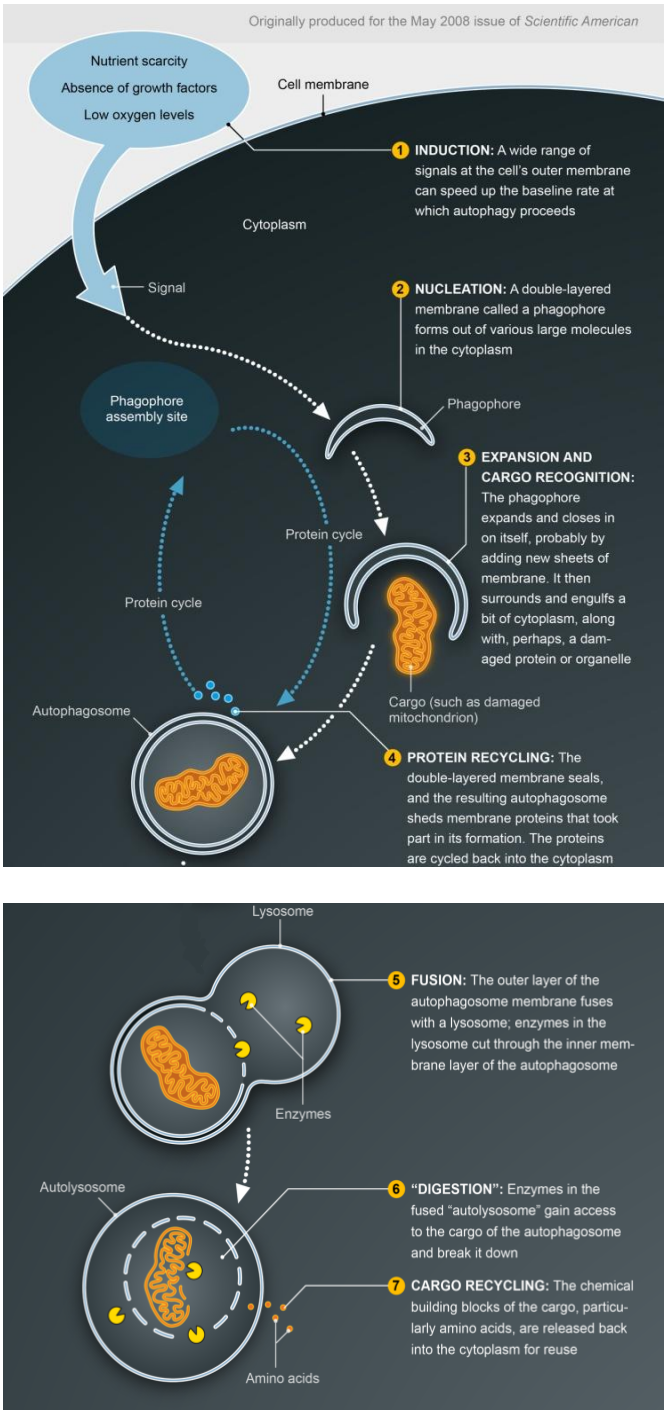

Figure 11. The process of autophagy can be divided into 7 steps: induction, nucleation, expansion and cargo recognition, protein recycling, fusion, digestion and cargo recycling[18]

The discovery of autophagy in yeast and subsequent studies in mutants that were deficient in the autophagy pathway resulted in a total of 31 Atg genes. Out of this, at least 18 genes encode the fundamental machinery for the synthesis of autophagosomes[25]. The map of the genes is as shown in (fig 12). Studies on Atg genes have revealed five distinct subgroups: Atg1 kinase and its regulators, Phosphatidylinositol(PtdIns) 3-kinase complex, Atg12 conjugation system, Atg8 conjugation system, and Atg2-Atg18 complex and Atg9. Atg gene knockdown has shown to accelerate rather than delay cell death showing that autophagy plays a protective role.[15,16,17,18]

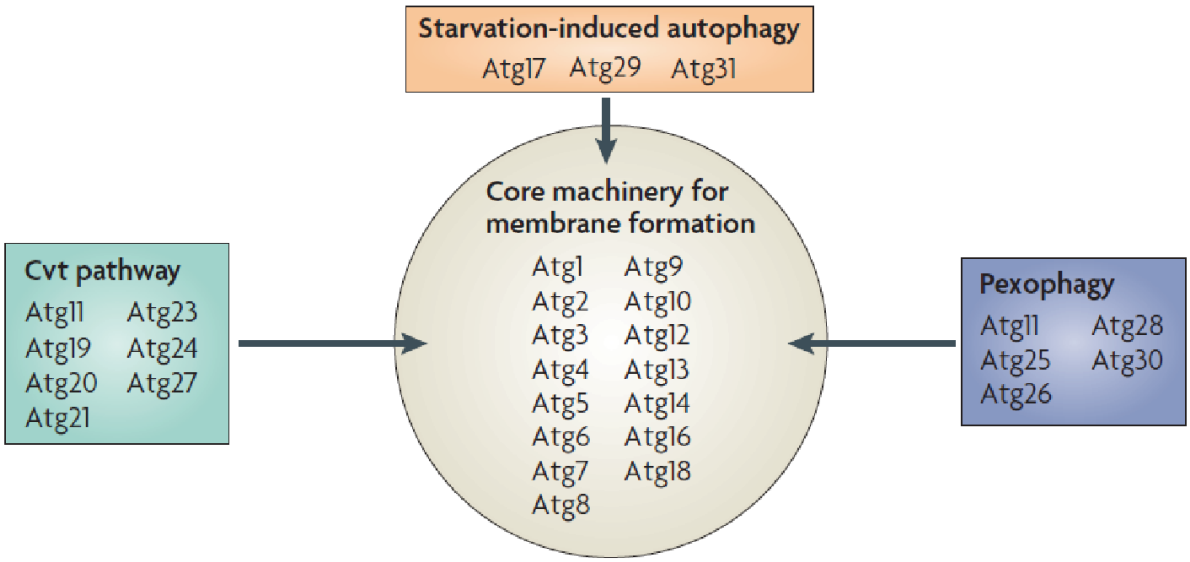

Figure 12. Map of Atg proteins. These proteins are commonly required for three pathways- starvation induced, cytoplasm to vacuole targeting pathway(Cvt) and pexophagy. Cvt mediates the transport of aminopeptidase from cytoplasm to vacuole. Pexophagy is the autophagic degradation pathway for peroxisomes in yeast[16].

Pre-autophagosomal Structure(PAS)

Upon induction of autophagy, the Atg proteins assemble at a site known as phagophore assembly site or PAS. Fluorescence microscopy showed one dot in close proximity to the vacuole in each cell. This dot represents the assembly of Atg proteins that are responsible for autophagosome formation (fig 13). Here, they coordinate with tethering factors and proteins called soluble N-ethylmaleimide-sensitive fusion (NSF) attachment protein receptors (SNARES) along with membranes derived from golgi, endoplasmic reticulum as well as mitochondria to form the autophagosome. Snares are transmembrane proteins that can assemble in complexes between two opposing membranes to mediate vesicular fusion events.[19,20] Atg proteins organize around the PAS according to hierarchical relationship among subgroups. Genetic deletion or removal of any of the Atg protein that is upstream in the hierarchy significantly affects the localization of downstream Atg proteins. Among Atg proteins in a subgroup, not only hierarchical but also interdependent relationships exist. Their hierarchy represents their order of action in formation of autophagosome[16]. This is schematically depicted in fig 14.

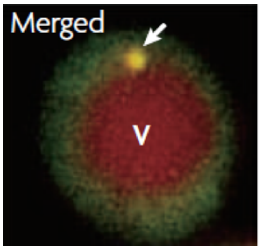

Figure 13. The arrow represents the PAS, assembly of Atg proteins. 'V' - vacuole[16]

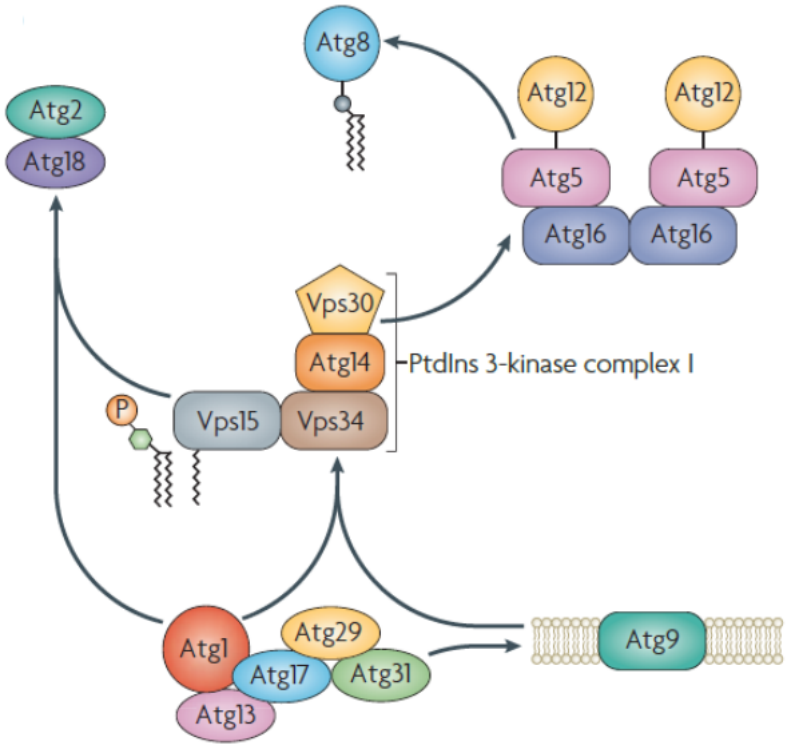

Figure 14. Hierarchical model of localization of Atg proteins to PAS[16].

Atg1 kinase

The Atg1 kinase and its regulators Atg13, Atg17, Atg29, Atg31 participate in the initial step of autophagosome formation and are most upstream in the hierarchy of Atg proteins in terms of their localization to PAS. Under conditions that induce autophagy, most Atg proteins lose their ability to localize at the PAS in absence of Atg17. This suggested that Atg17 is the most upstream in PAS organization. It is a scaffold protein that recruits other Atg proteins for PAS organization. No mis-localization was observed in the absence of Atg8 suggesting that Atg8 was located downstream with respect to other Atg proteins for PAS organization[21]. Atg1 is a serine/threonine protein kinase whose activity is enhanced largely following nutrient starvation[16].

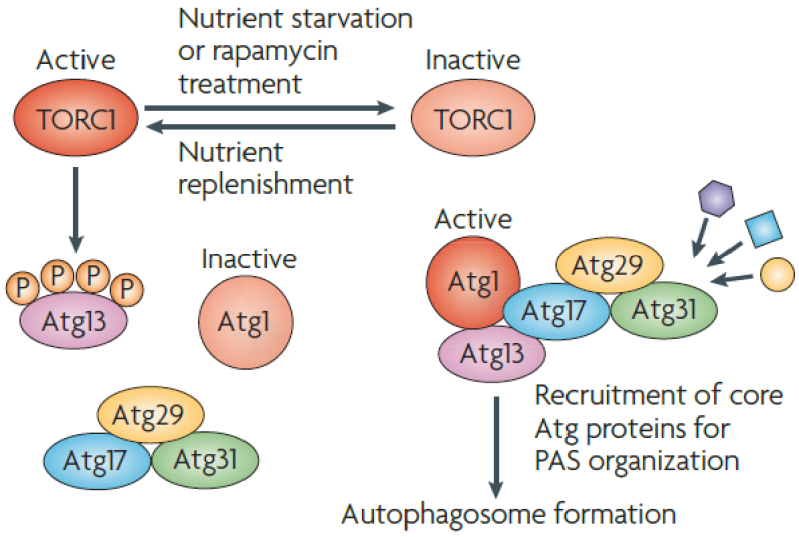

Figure 15. Initiation of Autophagosome formation. Under nutrient starvation conditions, TORC1 gets inactivated, Atg13 is dephosphorylated. The free Atg13 then associates itself with Atg1 and other proteins to the PAS to initiate autophagosome formation[16].

In normal conditions, Target of Rapamycin(TOR), a kinase that plays a significant role in cell cycle progression and in controlling translation is active and phosphorylates Atg13[22]. TOR is composed of two complexes- TORC1 and TORC2 of which TORC1 is sensitive to autophagy. When autophagy is induced, TOR is inhibited[16] (fig 15).

Phosphatidylinositol (PtdIns) 3-kinase complex

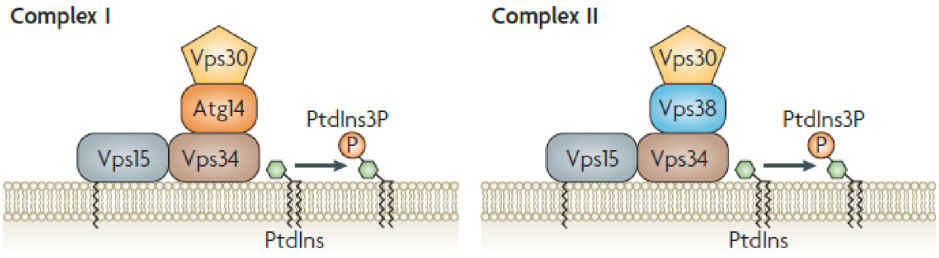

Figure 16. Phosphatidylinositol (PtdIns) 3-kinase complex. PtdIns 3-kinase consists of complex-1 and complex-2. Complex-1 is essential for autophagy and complex-2 is necessary for vacuolar protein sorting.

The Atg1 subgroup forms a complex with the PtdIns kinase also known as Vps34 that phosphorylates the D3 position of the inositol ring in PtdIns resulting in PtdIns3P as shown in (fig 16). PtdIns3P is necessary for autophagy and is responsible for recruiting effector proteins for autophagosome formation at the PAS. It is enriched in the inner surface of the isolation membrane and autophagosome as shown in (fig 17).

Vps34 forms two complexes- Complex1 is composed of Vps34(catalytic subunit), Vps15(regulatory subunit), Vps30(also known as Atg6, BECLIN[24]) and Atg14. Atg14 bridges Vps30 and Vps34 to form complex1. Complex2 consists of Vps38 instead of Atg14. Complex1 is essential for autophagy and Atg14 in complex1 helps to direct it to PAS[16,25]. Atg14 is required for localization of Atg2-Atg18 complex to the PAS. The formation of PtdIns3P by Vps34 kinase activity is essential as Atg18 binds to PtdIns3P and then the complex Atg18-Atg2 is recruited to the PAS for autophagosome formation[16]. Atg9 is the sole trans-membrane protein which has six trans-membrane domains with the amino and carboxy termini exposed to cytosol. Atg9 is known for its bi-directional movement between PAS and non-PAS structures/cytoplasmic pool and this movement is required for autophagosome formation. Atg9 shuttling helps to transport membrane to PAS[26]. Atg9 can self-associate as well as interact with Atg17 which is part of the Atg1 subgroup[16].

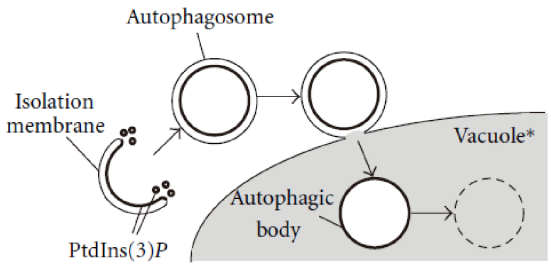

Figure 17. The converging site of PtdINs3P on the autophagosome[25]

Ubiquitin-Like Conjugation Systems

Two protein conjugation systems exist among the Atg subgroups each of which has two ubiquitin-like proteins and three enzymes**.** The proteins include Atg8 and Atg12 while the enzymes are Atg3,7 and 10.

Atg8 conjugation: Atg8 is synthesized as a precursor with an additional residue, Arg, in its carboxy terminus. This is cleaved by the cysteine protease Atg4 to expose the Gly residue**.** Atg7 and Atg3 are the E1 and E2 enzymes respectively. Atg7 enzyme functions like an E1 enzyme wherein it activates the exposed Gly of Atg8 and forms a thioester intermediate with its active Cys residue in a reaction involving ATP. Atg3 then receives the Gly residue of Atg8 at its active Cys residue and transfers it to the target substrate molecule which in this case is the amide bond with the amino group in the lipid phosphatidylethanolamine(PE)[16]. Atg8 is now in its lipidated form Atg8-PE and localizes almost to all the structures related to autophagy. This includes PAS, isolation membrane, autophagosome, the inner membrane that is released into the vacuole on fusion between the autophagosomal outer membrane and the vacuole and the outer membrane of the autophagosome. Atg8 forms oligomers when it conjugates to PE and this leads to aggregation of liposomes. The Atg8-PE conjugates on one membrane interacts with another membrane leading to tethering of the membranes and hemifusion. Hemifusion is the fusion of outer leaflets of two membranes that oppose each other with their inner leaflets left intact. This plays an important role in determining the size of autophagosomes as smaller autophagosomes were found in Atg8 deficient mutants that had issues with membrane tethering and hemifusion. Atg8-PE is also involved in closure of the isolation

membrane to form the autophagosome. Autophagosomes with abnormal morphology were reported in cells that were deficient in Atg8-PE conjugate formation[27]. Atg4 is also a deconjugation enzyme that cleaves Atg8 and releases it from membrane. This plays an important role in recycling Atg8 which can be used again in future to form membranes. Any part of Atg8 that is left behind in the autophagosome is degraded in the vacuole[16] (fig 18).

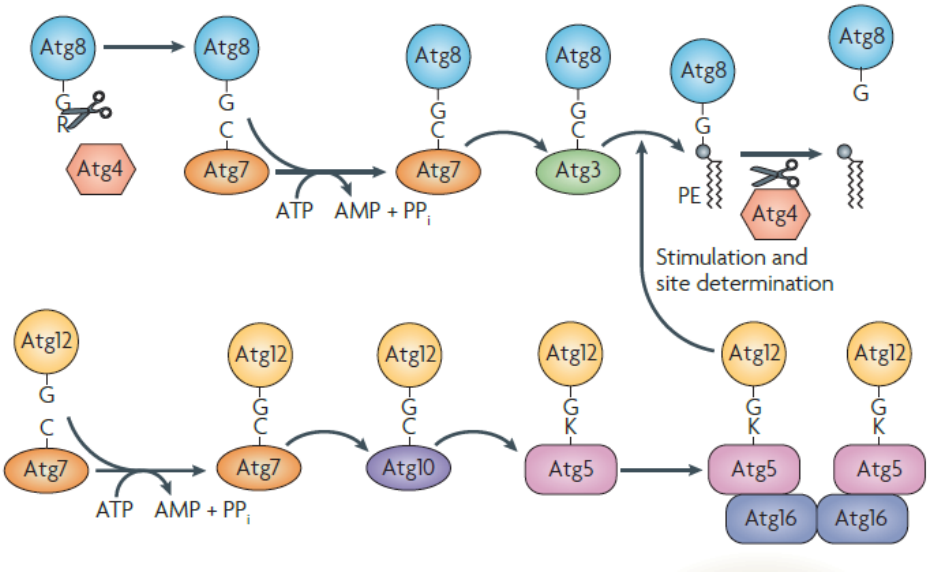

Figure 18. The Atg8(above) and Atg12(below)conjugation and deconjugation system[16]

Atg12 conjugation: Like the Atg8 system, Atg12 is cleaved by Atg7 which acts as the E1 enzyme exposing the C terminal Gly residue, and then it is acted upon by E2 enzyme, Atg10 and finally transferred to form an isopeptide bond with the lysine residue of Atg5. The Atg12-Atg5 conjugate then forms a complex with Atg16 on account of oligomerization ability of Atg16[16]. Atg12-Atg5 conjugates have been shown to enhance the formation of Atg8-PE. It functions like an E3 enzyme and directly interacts with Atg3.

Atg3, being an E2 enzyme has an E2 domain; it adopts an inactive conformation in absence of Atg12-Atg5 complex. The side chain of the catalytic cysteine residue faces away from the threonine residue. In presence of Atg12-Atg5 the cysteine residue is reoriented towards threonine causing an easy transfer of Atg8 to PE[27] (fig 19).

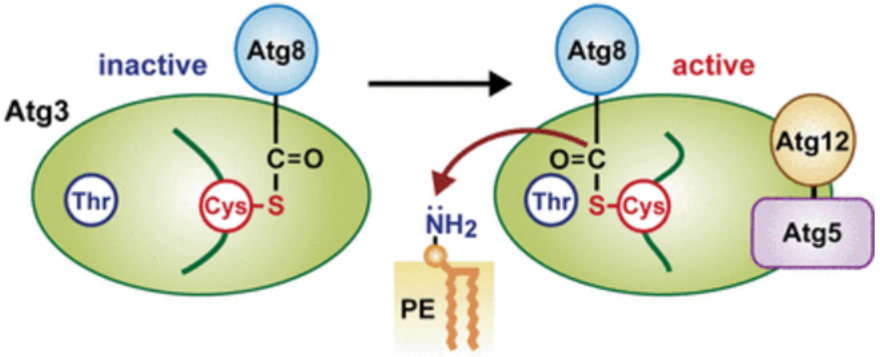

Figure 19. Presence of Atg12-Atg5 causes cysteine residue to reorient towards threonine thereby enhancing the activity of Atg3.

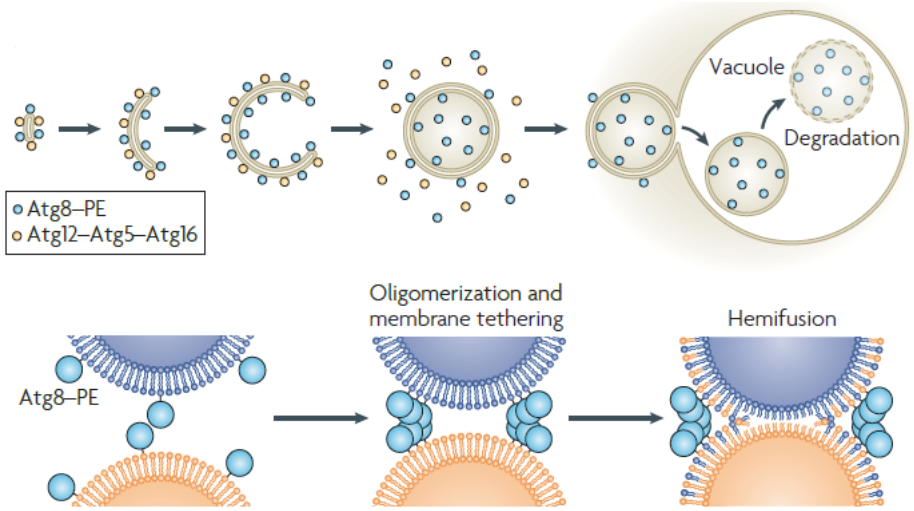

Figure 20. Localization of ubiquitin-like protein conjugates on autophagosomes

Unlike other ubiquitin systems, Atg12-Atg5 does not determine substrate specificity. The specificity is determined by Atg3 itself. Although Atg16 is required for Atg12-Atg5 to

function like E3 *in vivo*, it is not essential in *in vitro* settings[16]. There is no E3 enzyme for the Atg12 conjugation system. Here the E2 enzyme directly recognizes the substrate Atg5. The Atg12-Atg5-Atg16 complex is present only on the outer surface of the phagophore. The Atg8-PE is carried through the autophagosome into the vacuole where it is degraded. The Atg12-Atg5-Atg16 dissociates from the membrane once the autophagosome is formed (fig 20).

Tools and Technologies used to identify cell death

Cell death assays must answer two critical questions: Whether the cells in question die? If so, what is the pathway? They must be accurate and specific as the results of these assays are used for drug development[33]. Some of the techniques along with their benefits and drawbacks are listed below:

Light microscopy: Visual inspection by light microscopy is a simple and cost-effective technique, but can be non-specific and/or inappropriate for most experimental settings. This can be done on both live samples as well as histological sections. Morphological changes associated with dead cells can be visualized. This technique is however time consuming, operator-dependent and tends to underestimate fraction of live/dead cells. It also fails to identify completely disintegrated cells whose fragments are too small to be seen and cells in early stages of death as they do not display morphological modifications. This can be partially overcome by use of time-lapse video microscopy that will take account of cell death during entire duration of experiment. Vital dyes such as trypan blue and crystal violet can be used to identify dead cells that have not undergone significant

structural changes. However, these techniques are unsuitable for high throughput applications[33].

(Immuno)cyto(histo)chemistry protocols are suitable for quantification of cells that display some molecular processes related to death specifically those that can be detected by primary antibodies. Although this method can detect cells at early stages of death, it is totally dependent on performance of primary antibodies used and has low levels of throughput.

Terminal deoxynucleotidyl transferase-mediated dUTP nick-end labelling(TUNEL) assay has been used commonly for detection of apoptosis. This method works on the principle that DNA strand breaks during apoptosis and an enzyme Terminal deoxynucleotidyl transferase(TdT) catalyzes the labelling of these broken strands with dUTP which is then detected by immunoperoxidase staining[34]. This assay has limitations such as it is not specific to apoptosis, produces a lot of background and false positive staining make it difficult to reach conclusions[35]. Electron microscopy provides ultrastructural information and helps to visualize ultrastructural modifications such as gaps in plasma membrane, mitochondria swelling, chromatin condensation etc. But it is not a robust quantitative approach; this technique can be laborious and requires trained personnel.

Fluorescence microscopy: The use of fluorescence has several advantages over the above techniques in terms of a) better signal to noise ratio b) the detection method does not involve any enzymes whose efficiency could be affected by other variables such as pH, temperature etc. c) secondary antibodies can be coupled to fluorochromes and detected by

staining events; this allows detection of multiple cell death related events at the same time d) finally, fluorescent dyes and fluorescent fusion proteins can be used along with the above immunological methods to study cell death related parameters. The applications with regards to cell death include quantification of cells with caspase activation, detection of mitochondrial permeability, analysis of localization of pro-apoptotic proteins, translocation of intermembrane space proteins of the mitochondria. It has limitations such as auto-fluorescence which reduces signal to noise ratio, inability to observe simultaneously labelled and unlabeled structures, absolute requirement for visual quantification of cells under study in order to obtain quantitative data from the fluorescence microscopy. But most of these limitations have been overcome with availability of high throughput workstations that help in simultaneous and automated imaging of 96 well plates as well as optimization in software that allows for image reconstitution and analysis.

Spectrophotometry: End-point determination of cell death can be done by spectrometric quantification of formazan using MTT assay. This method has advantages such as rapidity, ability to process large number of samples, being economical and not requiring any special laboratory equipment. But the release of LDH cannot be used to distinguish between different cell death pathways and the release of enzyme can be affected by several variables including pH, specific components in the culture medium. Metabolic alterations such as excessive cell density and overconsumption of media can affect the conversion of MTT/WST-1 by enzymes which may not correlate with number of viable cells. These techniques are only meant to be used to detect early phase of cell death when thousands of conditions must be screened along with suitable controls.

Enzyme linked immunosorbent assays(ELISA) kits can be used to measure cell death related parameters in intact cells, cell culture supernatants, body fluids, tissue extracts and subcellular fractions. But it requires excessive preprocessing of samples and all ELISA detectable markers decay making it impossible to draw any correlation between the marker and dead cells[33].

Immunoblotting: Immunoblotting alone or along with immunoprecipitation can be used for qualitative or semi-quantitative analysis of cell death phenomena including activation of cell death regulators, caspase activation, cleavage of caspase substrates, translocation of IMS proteins to extramitochondrial space, conformational changes in pro-apoptotic Bcl-2 protein family members. However, these procedures are time consuming, not suitable for large scale applications and provides reliable results only when primary antibodies are at sub-saturating concentrations. Immunoblotting is not suitable for heterogenous cell samples such as primary tissues or solid tumors. It is ideal for subcellular fractions[33].

Cytofluorometry is suitable for studying cell death on a per cell basis. It can be used to detect morphological changes that characterize apoptosis. Cytofluorometer can provide quantitative results that makes it free from operator bias. It can also capture 10-10000 events rapidly from samples contributing to a high throughput and increased statistical power. But the need for large number of cells makes it unsuitable for study of primary cell cultures. As this method requires cell to cell dissociation, it is also unsuitable for histological sections. Luminometry is used for quantification of intracellular bioenergetic stores and hence is applied to cell death research. This technique is not reliable as ATP/ADP ratio can vary due to intracellular and extracellular interferences[33].

Biosensors for detecting Cell Death

The term 'biosensor' appeared in scientific literature in the late 1970's[36]. Biosensors are molecular entities or devices that enable bio-sensing. Bio-sensing includes a diverse array of techniques used to generate an experimentally accessible 'read-out' of molecular interaction between a biomolecule derived molecular recognition element(MRE) (such as protein domain) and an analyte of interest (such as small molecule or another protein or enzymatic activity). The efficiency of the biosensor lies in its ability to transduce a nanometer scale event such as a molecular recognition process into an observable property such as fluorescence or hue. Nanometer scale events could be either a change in the distance between MRE and analyte or a change in conformation of the MRE. Genetically encoded biosensors allow non-invasive imaging of the specific biochemical process while simultaneously preserving spatial and temporal information. Aequorea green fluorescent protein (FP) and its engineered variants are a critical part of these genetically encoded biosensors owing to its photo-physical properties. FP based biosensors have a plethora of benefits including a) they are easy to construct by standard molecular biology techniques b) they can be non-invasively introduced into living cells where the cellular machinery can produce them by transcription and then by translation c) able to be targeted to most cellular components using specific signal sequence tags d) able to provide information about the biomolecular process in the natural habitat of the protein. Additionally, both temporal and spatial information is preserved in this process[37]. Biosensors can be based on 1) intermolecular Förster Resonance Transfer Energy (FRET) 2) intramolecular FRET

Intermolecular FRET based biosensors: This group is basically a split construct where the MRE is fused to one of the FP protein and the analyte protein is fused to the other protein. This design is useful to study protein-protein interactions (fig 21).

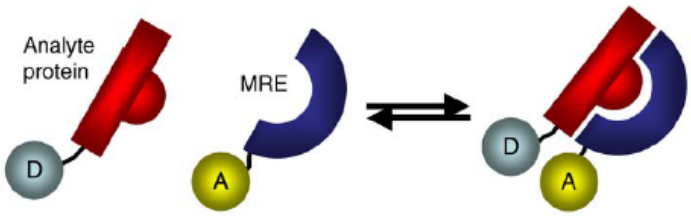

Figure 21. Intermolecular FRET based biosensor. This biosensor is used to detect protein-protein interactions where each of the protein is tagged to each of the FP of the FP pair and change in donor and acceptor intensities are measured.

Intramolecular FRET based biosensors: consists of two FPs flanking an MRE (fig 22a). Change in conformation of MRE triggers a change in distance between the two FPs thereby affecting FRET efficiency. This biosensor design has been used to detect proteolytic activity, post-translational modifications(PTM) and small molecules. A MRE to detect proteolytic activity consists of a polypeptide as substrate which is cleaved by a protease. The conformation of a successful cleavage comes from a decrease in FRET signal along with an increase in donor signal (fig 22b). MRE to detect PTM activity consists of a polypeptide substrate specific for the PTM activity along with a binding domain that preferentially binds to the modified substrate. Both the substrate and binding domain change conformation post PTM activity (fig 22c). Fig 24d shows a MRE that changes conformation in presence of an analyte.

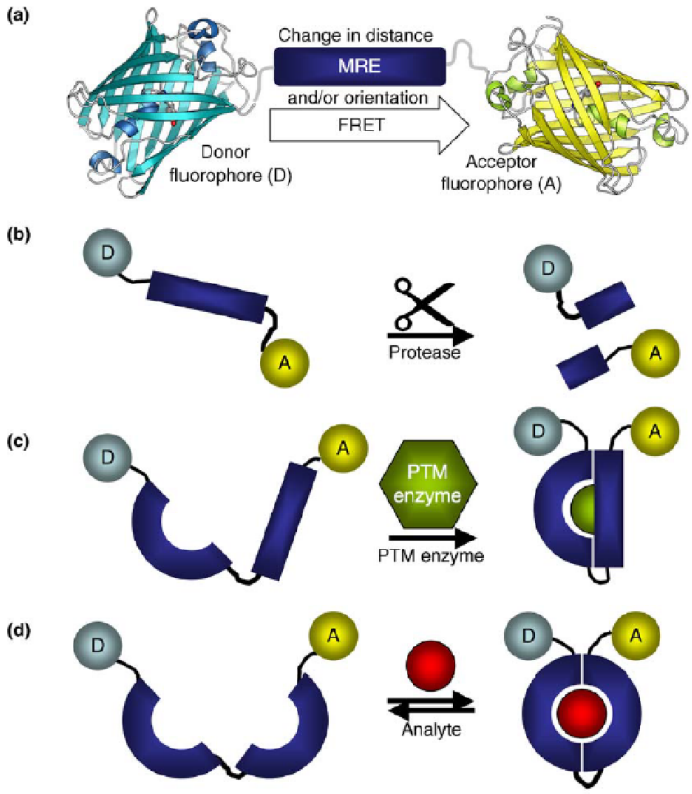

Figure 22. Intramolecular FRET-based Biosensor. a) the basic intramolecular biosensor design b) sensor to detect proteolytic activity c) an MRE capable of detecting PTM and d) change in conformation of proteins on binding to small molecule analytes[37].

The use of biosensors is slowly replacing other immunological techniques because of its compactness, portability, high specificity and sensitivity. The use of chemical synthesis method to develop sensors for biologically relevant analytes was challenging. Some of these limitations were overcome by using proteins and enzymes as components of sensors for biochemical analytes. Various proteins have wide range of selective affinities incorporated into them by evolution. The number of ligands recognized by the proteins is extremely large and ranges from small molecules to macromolecules, including proteins themselves. Choosing proteins as components of sensors has several advantages including low cost involved in design and synthesis, the fact that proteins in general are soluble in

water and the possibility of changing/improving some of the properties of proteins by genetic manipulation. With the application of site-directed mutagenesis, new positions can be inserted for reporter labeling, amino acid sequences can be altered and protein-binding constants can be modified. Optical methods of detection such as fluorescence energy transfer, polarization and solvent sensitivity has allowed to construct stable and robust devices as well as improved signal to noise ratio[36].

Förster resonance energy transfer (FRET)

FRET is a physical phenomenon that relies on close interaction between two fluorophores called the donor and acceptor. A donor fluorophore in its excited state may transfer energy to an acceptor molecule through nonradiative dipole-dipole coupling. Consequently, the donor fluorescence is quenched and acceptor molecule is excited. Energy is lost without emission of photon, either by heat or fluorescence emission (fig 23).

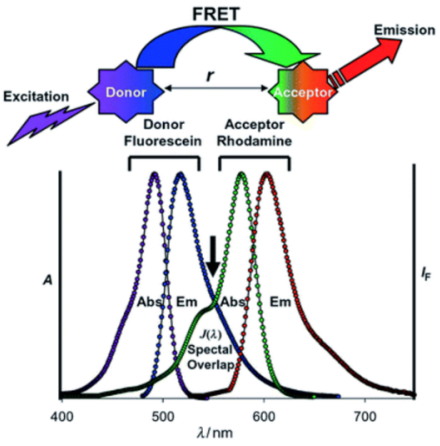

Figure 23. Schematic representation of FRET. An excited donor transfers energy to acceptor that emits it through fluorescence in a non-radiative fashion. Also seen is the absorption and emission profile of a commonly used FRET pair: donor fluorescein and acceptor rhodamine.

FRET does not occur if the distance between the fluorophores exceeds 10nm. The rate of transfer for a donor and acceptor separated by a distance can be expressed in terms of the Förester distance (R_0) which is the distance between donor and acceptor at 50% energy transfer efficiency (fig 24). The efficiency of this energy transfer is inversely proportional to sixth power of distance between donor and acceptor. This makes FRET highly sensitive to changes in distance[38,39,40]. It is this dependence on distance that makes FRET technology able to study molecular interactions on a 1-10nm scale. When the distance of the donor and acceptor narrows from R_0 to $0.5R_0$, the efficiency of FRET increases from 50% to near maximum. On the other hand, when the donor-acceptor distance increases by 100% of R_0, FRET efficiency decreases to an almost undetectable level of 1.5%.

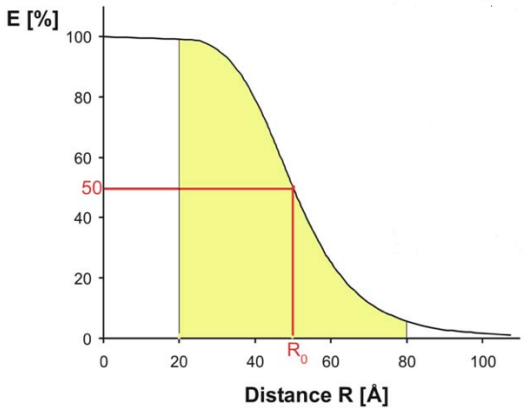

Figure 24. Sensitivity of FRET to changes in distance. Measuring E provides a sensitive indication of the change in D–A distance around the Förster distance, as seen by the relationship between the distance and the E of a single D–A pair, given its Förster distance of 50Å.

The requirements for a donor and acceptor to be an ideal FRET pair include a) distance of less than or equal to 10nm between the donor and acceptor b) an overlap between the donor

emission spectrum and acceptor absorption spectrum and c) Molecular dipole moments of donor and acceptor should be aligned for efficient energy transfer[41](fig 25).

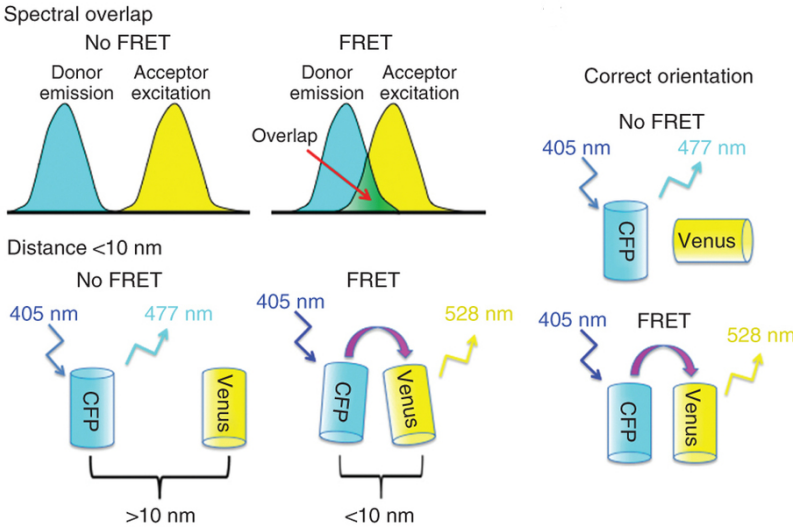

Figure 25. the three primary requirements for a pair of fluorophores to be an ideal FRET pair[42]

The high sensitivity of this technology serves as the basis of two types of FRET-based applications: FRET can be used as a spectroscopic ruler to precisely measure molecular distance when the donor and acceptor distance is not far from their R_0; the "on" and "off" status of FRET can be monitored to determine the status of molecular interaction.

Quantification of sensitivity and efficiency of a FRET biosensor is achieved by studying the kinetics of the enzyme-substrate pair. This typically involves monitoring the molecular processes over a period of time such as binding of ligand to receptor, enzyme cleaving substrate, protein-protein dynamics etc. The assays used to study these processes are called kinetic assays and I have developed one such assay to study the action of enzyme protease Atg4A on substrate Gate-16.

Kinetic Assays

Proteases are important drug targets. A simple search using the NIH PubMed server will find hundreds of thousands of proteases related articles. Proteases play critical roles in multiple biological pathways - the human genome sequencing project revealed that ~2% of our genes encode proteases - and are implicated in many diseases, including infectious diseases, inflammation, cancer, degenerative diseases, and many others[62]. Robust biochemical assays such as the enzyme kinetic assays reveal structure-function relationships that are essential for drug development.

Atg4 is a cysteine protease that is known to cleave Atg8 family proteins so that they conjugate to phospholipids, a process that is very essential for autophagosome biogenesis. This makes Atg4 an important target to modulate in the Autophagy pathway. While only one Atg4 is present in yeast there are four Atg4 homologues in human and mouse, each of which has different substrate specificities and catalytic efficiencies. The homologues include Atg4A, Atg4B, Atg4C and Atg4D. There are eight human Atg8 homologues belonging to two subfamilies: 1) the LC3 (microtubule-associated protein 1 light chain-3) subfamily which includes LC3A, LC3B AND LC3C and 2) GABARAP (GABAA receptor-associated protein including GABARAP, GABARAPL1/Atg8L/GEC1, GABARAPL2/GATE-16/GEF2, and GABARAPL3). The conserved cleavage site of Atg4 is common for all the substrates. Studies have shown that Atg4B is able to cleave most of the human Atg8 homologues. But Atg4A is a protease only for the GABARAP family, not the LC3 subfamily. For the purposes of this study, we will concentrate on the Atg4A protease and the Gate16 or GABARAPL2 substrate[63].

CHAPTER 2

DEVELOPMENT OF FRET BASED BIOSENSORS TO DETECT APOPTOSIS AND AUTOPHAGY

Abstract

Based on morphological alterations, the most fundamental cell death processes include Apoptosis, Autophagy and Necrosis. Any other cell death pathway is a form of one of these that is induced with different triggers. A disruption in the balance among any of these has been implicated in several diseases. To better understand these diseases, it is necessary to gain an in-depth knowledge of the underlying mechanisms of the cell death pathways. There is a significant need to have a very specific and sensitive technology to identify cell death pathways in different situations such as to understand the etiology and prognosis of a disease, the effect of treatment with certain drugs among many others. Förster resonance energy transfer (FRET) technology has been widely used in biological and biomedical research. This powerful tool can elucidate protein interactions in either a dynamic or steady state and is very sensitive to small changes in distance (of the order of 10^6). Here, we demonstrate a very sensitive and quantitative way of identifying Apoptosis and Autophagy in an *in vitro* system such as e.coli using FRET. The method involves the design of genetically encoded Biosensors that consists of a protein of interest fused between fluorescent proteins- Cypet and Ypet. The sensor is based on enzyme substrate principles and relies on rapid detection of loss of FRET signal in the event of Apoptosis and Autophagy. The sensor is highly effective owing to use of a FRET pair such as Cypet-Ypet that promises high quantum yield, extinction coefficient and enhanced dynamic range,

along with a robust construct design and use of a sensitive technology such as FRET. This sensor can also be transfected into different cell lines to identify and differentiate between apoptosis and autophagy when the cells are treated with drugs/inhibitors.

Introduction

Apoptosis is described as a cell intrinsic suicide program characterized by definite morphological features. The features include cell shrinkage, chromatin condensation, membrane blebbing and formation of apoptotic bodies[3,4,7]. Depending on the nature of trigger, apoptosis can be either extrinsic or intrinsic. Both the mechanisms converge in activation of caspase cascade where upstream caspases proteolytically cleave downstream caspases that inturn cleave a large number of essential proteins required for cell survival executing the cell death[52].

Autophagy is a catabolic degradation of cellular components where in the organelles and cytoplasmic components are delivered to lysosomes for degradation. Autophagy is a very interesting and important pathway to follow owing to its dual role in several diseases. For instance, in cancer it is known in some cases to exacerbate the disease while in other cases to ameliorate the symptoms. Studies have also revealed cross talks between apoptosis and autophagy that indicate that Apoptosis is the default pathway chosen by cells when triggered to die. This also raises the need to differentiate between the two pathways and find a very specific and sensitive technology to do that.

Fluorescent Biosensors are among a highly diverse class of biosensors that exploit the intrinsic property of a biomolecule to modulate the fluorescent intensity or hue of a pair of fluorophores. The Biosensors have advantages of high sensitivity, versatility and

simplicity. Most of the fluorescent protein biosensors have applications in cells that are in culture, tissue or whole animals. A very promising application of the biosensors has been in the creation of polypeptides that have the sensing domain fused between the donor fluorescent protein and acceptor fluorescent protein. The sensing domain has two essential functions: it must provide the specificity of the biosensor to the biochemical signal of interest and second, the response to the biochemical signal must be a change in conformation that effectively modulates the FRET efficiency between the two fluorescent proteins. Ideally the change in FRET efficiency must be large enough to ensure a high change in intensity ratio I_a/I_d where I_a and I_d are the fluorescent intensities in acceptor and donor emissions upon donor excitation.

Several biochemical and fluorescent methods have been used to identify apoptosis including imaging of cells to visualize alternations in membrane, DNA fragmentation, TUNEL assay, time lapse microscopy, DNA end labelling techniques and flow cytometry.[52,53,54,55]. Most of these methods are also used to monitor autophagy[60,61]. All of these methods have some limitations and drawbacks. For instance, microscopy based methods have problems such as inability to quantify data, error prone observations, lack of reproducibility and laborious procedures. Other techniques such as flow cytometry have limitations such as requirement of large number of cells, lack of specificity and labelling of proliferating cells in case of DNA nick-end labelling technique[1,2,56]. With the advent of fluorescent techniques, FRET has been used as a popular method to study apoptosis and autophagy[57,58,59]. Protease assays are commonly used by exploiting FRET technology or by electrophoretic methods. The SDS-PAGE electrophoretic method although convenient

does not lend itself to quantitative analysis very easily and has limitations owing to the slow signal detection of the method[45,46]. Despite efforts to use fluorescent protein based biosensors, there have been no reports in literature on the use of the FRET pair Cypet-Ypet to monitor apoptosis. Cypet-Ypet pair was evolutionary evolved from ECFP-YFP and has high quantum yield, high extinction coefficient and better dynamic range making it very attractive for a wide range of applications[43].

Here we report the development of FRET based biosensors that is highly sensitive and specific to the detection of Apoptosis and Autophagy. The Apoptosis sensor Cypet-DEVD-Ypet as well as the autophagy sensor Cypet-LC3B-G16-Ypet were developed using standard restriction enzyme based cloning strategies. While the apoptosis sensor did yield the desired result, the autophagy peptide sensor did not. To overcome the problem, Autophagy sensor Cypet-Gate16-Ypet was developed with the full length Gate-16 protein using seamless cloning techniques. The design and schematic of the sensors are depicted in (fig 26), (fig 27) and (fig 28). Both the sensors can detect Apoptosis and Autophagy in an *in vitro* system within 1 hour. The sensors can be used to develop quantitative data such as enzyme efficiency parameters of caspase involved in Apoptosis and Atg4A in Autophagy. The FRET based protease assay can be converted to high throughput assay to look for small chemical compounds that can specifically inhibit the enzyme activity. This will be a major step towards better understanding of the cell death pathway.

Apoptosis: Substrate design

A)

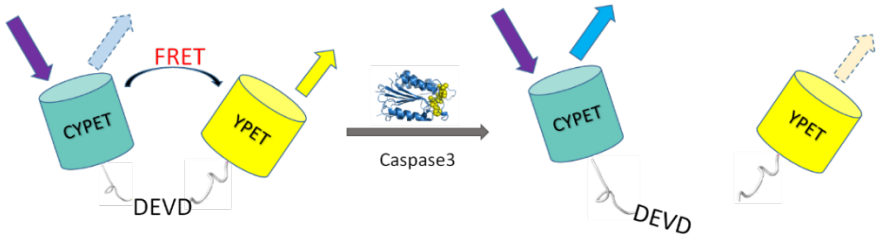

B)

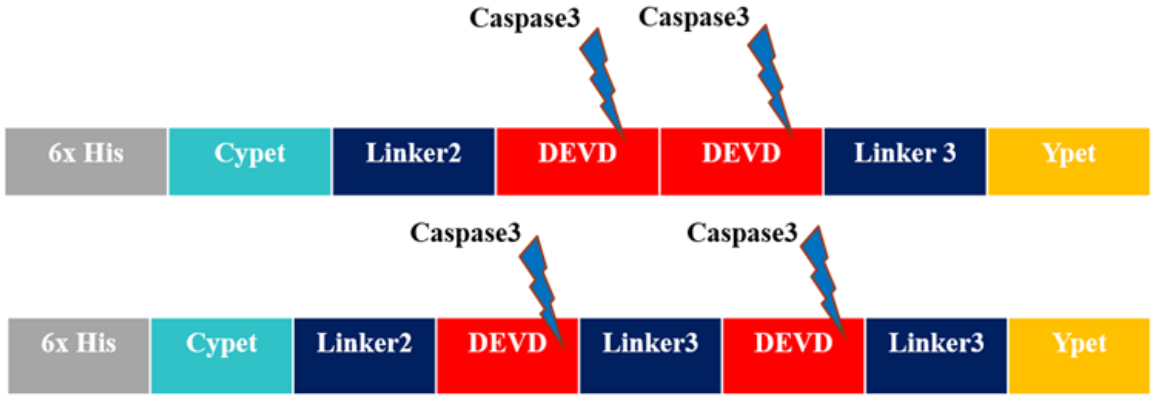

Linker2 : TSGSPGLQEFGT, Linker3: LAAALAAA

Figure 26. A) The cartoon depicts the principle behind the sensor design. In absence of Apoptosis, a strong FRET signal can be observed. When caspase-3 is added, it cleaves DEVD resulting in loss of FRET signal thus depicting Apoptosis. B) shows the design of Apoptosis biosensor. One design involves the presence of linker in between the peptide DEVD while the other has two peptide sequences DEVD in tandem. The construct is cloned into Pet28b vector with a N-terminal Histidine tag. Caspase-3 cleaves the Asp residue at P1 position of the DEVD peptide.

Autophagy: Peptide Design

A)

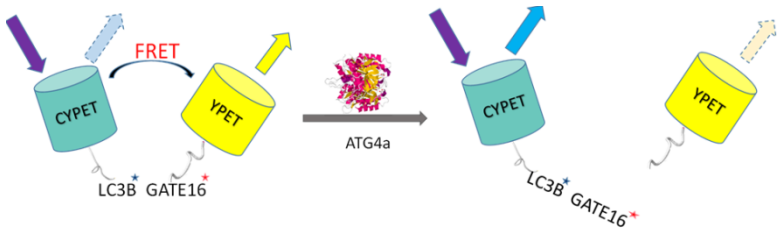

B)

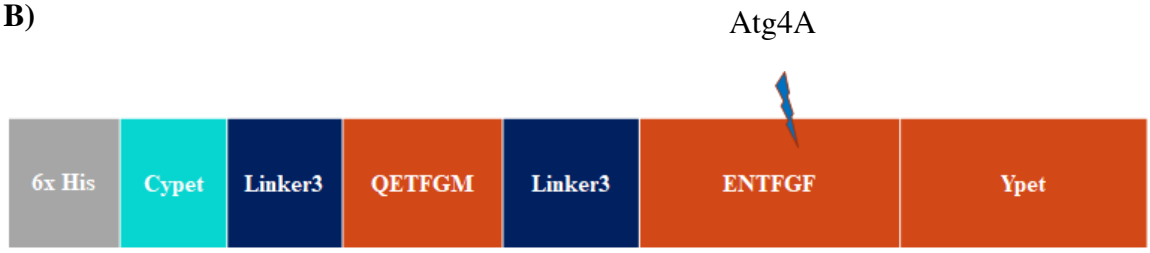

Figure 27. A) The cartoon depicts the principle behind the sensor design. In absence of Autophagy, a strong FRET signal can be observed. When Atg4A is added, it cleaves Gate16 peptide sequence at the Glycine Residue resulting in separation between Cypet and Ypet and loss of FRET. B) shows the design of Autophagy biosensor. Linkers are inserted in between LC3B and Gate16 peptide sequences and also at the N-terminus of LC3B sequence. The construct is cloned into Pet28b vector with a N-terminal Histidine tag. Atg4A cleaves the Gate-16 peptide at the C-terminus of glycine residue.

Autophagy: Full length Substrate Design

A)

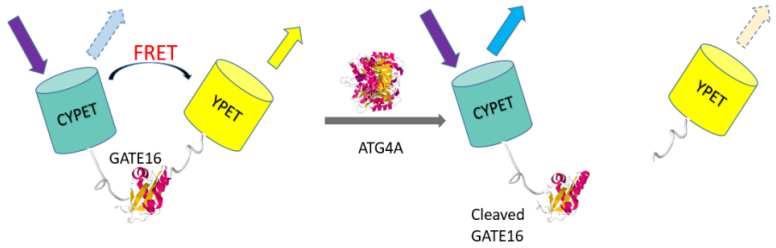

B)

Figure 28. A) The cartoon depicts the principle behind the sensor design. In absence of Autophagy, a strong FRET signal can be observed. When Atg4A is added, it cleaves Gate16 at the Glycine Residue resulting in separation between Cypet and Ypet and loss of FRET. B) shows the design of Autophagy full length Biosensor. Gate-16 full length sequence is sandwiched between fluorescent proteins Cypet and Ypet. The construct is cloned into Pet28b vector with a N-terminal Histidine tag. Atg4A cleaves Gate-16 at the C-terminus of glycine residue.

Materials and Methods

Plasmid Constructs

Apoptosis -

The open reading frame of Ypet was amplified using primers containing Sal1 and Not1 sites. The peptide sequence DEVD was used in tandem and augmented by PCR with primers containing SalI and NotI sites. Linker3 (LAAALAAA) was incorporated at the C-terminus of DEVD as part of the oligonucleotide primers. A construct Nhe1-Cypet-Linker2-Sal1-SUMO-Not1 developed previously by a graduate student was used. SUMO

fragment was digested out of this construct and the PCR product Sal1-DEVD-DEVD-Linker3-Ypet-Not1 was ligated into it. The resulting DNA fragment Nhe1-Cypet-Linker2-Sal1-DEVD-DEVD-Linker3-Ypet-Not1 was cloned into pCRII-TOPO vector (Life Technologies, Carlsbad, CA). After the sequence was verified, the insert was digested out of TOPO and cloned into Pet28b vector ((Millipore Corporation, Billerica, MA) with His tag at the N-terminus.

In another design version, Linker3 was incorporated between the two DEVD sequences. The method used to develop the construct was essentially the same as above. The resulting DNA fragment Nhe1-Cypet-Linker2-Sal1-DEVD-Linker3-DEVD-Ypet-Not1 was cloned into pCRII-TOPO vector (Life Technologies, Carlsbad, CA). After the sequence was verified, the insert was digested out of TOPO and cloned into Pet28b vector ((Millipore Corporation, Billerica, MA) with His tag at the N-terminus. Caspase-3 Gene was purchased from Addgene.

Autophagy- Peptide

The open reading frame of CyPet was amplified using primers containing HindIII and SalI sites, and Ypet was amplified using primers containing Sal1 and Not1 sites. The peptide sequences of human protein LC3B (QETFGM) and Gate16 (ENTFGF) were augmented by PCR with primers containing SalI and NotI sites. Linker3 (LAAALAAA) was incorporated at the N- and C- terminus of LC3B sequence as part of the oligonucleotide primers. The two DNA fragments HindIII-Nhe1-Cypet-Linker3-Sal1 and Sal1-LC3B-Linker3-Gate-16-Ypet-Not1 were cloned into pCRII-TOPO vector (Life Technologies, Carlsbad, CA). After their sequences were verified, the TOPO vector with the DNA

fragment, Sal1-LC3B-Linker3-Gate-16-Ypet-Not1 was linearized by digesting at Hind3 and Sal1 sites. HindIII-Nhe1-Cypet-Linker3-Sal1 was then digested out of the TOPO vector and ligated into the linearized TOPO vector at the N-terminus of the fragment Sal1-LC3B-Linker3-Gate-16-Ypet-Not1. After the sequences were confirmed, the cDNAs encoding fusion proteins were digested with NheI/NotI and cloned into the NheI/NotI sites of the pET28 (b) vector (Millipore Corporation, Billerica, MA). The plasmid encoding the Atg4A gene was purchased from Addgene.

Autophagy- Full Length

The open reading frame of CyPet was amplified using primers containing the portion of Pet28b vector sequence 3' to Nhe-1 site and Cypet as template, Ypet was amplified using primers containing the reverse complement of the portion of Pet28b that was 3' to Xho-1 site and Ypet as template. The open reading frame of Gate-16 was amplified using Gate-16 as template. The construct was designed to have three restriction enzyme sites Xho-1, Hind-III, Sal-1 in the same order from the C-terminus of Cypet to the N-terminus of Gate-16. Three more restriction sites Bamh-1, Nhe-1 and Ecor-1 were added in the same order from C-terminus of Gate-16 to the N-terminus of Ypet. Multiple restriction sites were incorporated so that the construct could be put to good use by future students in the lab. PCR was performed to amplify fragments Pet28b(overlap)-Cypet-Xho1-HindIII-Sal1, Gate-16-Bamh1-Nhe-1-Ecor-1 and Ypet. The concentration of the PCR fragments along with the digested vector fragment was measured using Nanodrop. The fragments were incubated with 10ul NEB Master Mix in a 1:1 ratio for 1 hour at 50˚C. The mixture was

then transformed into TOP10 Escherichia cells and the colonies screened to get the positive clone. The construct was obtained after sequencing results were confirmed.

Protein Expression and Purification

Apoptosis

BL21 Escherichia coli cells were transformed with Pet28b vectors encoding Nhe1-Cypet-Linker2-Sal1-DEVD-Linker3-DEVD-Ypet-Not1 as well as Nhe1-Cypet-Linker2-Sal1-DEVD-DEVD-Ypet-Not1 (hereafter will be referred as Cypet-DEVD-Linker3-DEVD-Ypet and Cypet-DEVD-DEVD-Ypet). The transformed bacterial cells were plated onto LB agar plates containing 50 mg/ml kanamycin, and a single clone for each protein was picked up for starter culture and inoculated in 10ml LB overnight at 37°C. This was transferred to 1L 2XYT medium and grown at 37°C for 3 hrs until optical density of the bacterial culture reached 0.5-0.6. Expression of polyhistidine-tagged recombinant proteins was induced with 0.3mM isopropyl b-D-1-thiogalactopyranoside at 25˚C overnight. The 6xhistidine-tagged recombinant proteins were purified from bacterial lysates with nickel agarose affinity chromatography (Qiagen, Valencia, CA, USA) and eluted in 20 mM Tris-HCl, pH 7.4, 50 mM NaCl, 1 mM DTT. Protein purity was examined by SDS-PAGE, and concentrations of the purified proteins were determined by the Bradford assay (ThermoFisher Scientific, Waltham, MA, USA).

Autophagy- Peptide

BL21 Escherichia coli cells were transformed with Pet28b vectors encoding Cypet-Linker3-LC3B-Linker3-Gate16-Ypet and Atg4A. The transformed bacterial cells were

plated onto LB agar plates containing 50 mg/ml kanamycin, and a single clone for each protein was picked up for starter culture and inoculated in 10ml LB overnight at 37°C. This was transferred to flasks of 1L 2XYT medium and grown at 37°C for 3 h until optical density of the bacterial culture reached 0.5-0.6. Expression of polyhistidine-tagged recombinant proteins was induced with 0.6mM isopropyl b-D-1-thiogalactopyranoside at 25˚C overnight. The 6xhistidine-tagged recombinant proteins were purified from bacterial lysates with nickel agarose affinity chromatography (Qiagen, Valencia, CA, USA) and eluted in 20 mM Tris-HCl, pH 7.4, 50 mM NaCl, 1 mM DTT. Protein purity was examined by SDS-PAGE, and concentrations of the purified proteins were determined by the Bradford assay (ThermoFisher Scientific, Waltham, MA, USA).

Autophagy-Full Length

BL21 Escherichia coli cells were transformed with Pet28b vectors encoding Cypet-Xho-1-HindIII-Sal-1-Gate-16-Bamh1-Nhe-1-Ecor1-Ypet (hereafter will be referred as Cypet-Gate16-Ypet). The transformed bacterial cells were plated onto LB agar plates containing 50 mg/ml kanamycin, and a single clone for each protein was picked up for starter culture and inoculated in 10ml LB overnight at 37°C. This was transferred to 1L 2XYT medium and grown at 37°C for 3 hrs until optical density of the bacterial culture reached 0.5-0.6. Expression of polyhistidine-tagged recombinant proteins was induced with 0.3mM isopropyl b-D-1-thiogalactopyranoside at 25˚C overnight. The 6xhistidine-tagged recombinant proteins were purified from bacterial lysates with nickel agarose affinity chromatography (Qiagen, Valencia, CA, USA) and eluted in 20 mM Tris-HCl, pH 7.4, 50 mM NaCl, 1 mM DTT. Protein purity was examined by SDS-PAGE, and concentrations

of the purified proteins were determined by the Bradford assay (ThermoFisher Scientific, Waltham, MA, USA).

Caspase Purification

In my first attempt to purify Caspase-3, standard purification protocol was followed as detailed above. But the yield was low and the resulting caspase was not able to cleave DEVD to demonstrate apoptosis. Caspase-3 was assumed to be toxic to the cells and that was the reason for the failure. In my second attempt, expression of caspase-3 was induced for 3 hours. But it did not yield a successful result. On a survey of scientific literature, I discovered methods used by other scientists to overcome the toxicity of caspase-3. I tried two of the methods that appeared straightforward to me. One method employed the use of induction for 2 hours along with the use of protease inhibitors and the other method induced for 1 hour. The former method did not work because it inhibited cysteine proteases as well. The second method helped to achieve the desired result. This was because caspase existed as its inactive zymogen, pro-caspase and got automatically proteolyzed to caspase only when induction was carried out for 3 or more hours. Since induction was done only for 1 hour, pro-caspase was purified as is. It did not convert to caspase-3. The resulting protein had high concentrated and good yield was obtained.

Results

Apoptosis FRET Assay

CyPet-DEVD-Ypet (2uM) was mixed with pro-caspase3 in a 1:1 molar ratio along with a suitable buffer (50 mM Hepes Ph 7.4, 1mM EDTA, 100mM NaCl, 10mM DTT,

10%glycerol,0.1% Chaps) for a total volume of 60ul and incubated for 60 min at 37°C. To serve as control, the substrate CyPet-DEVD-Ypet was mixed with the same buffer to a total volume of 60ul and incubated at the same temperature for the same time. The mixture was transferred to a 384 well plate and readings were taken from Flexstation II (Molecular Devices Inc) by providing excitation signals at 414nm.

Induced overnight at 25°C

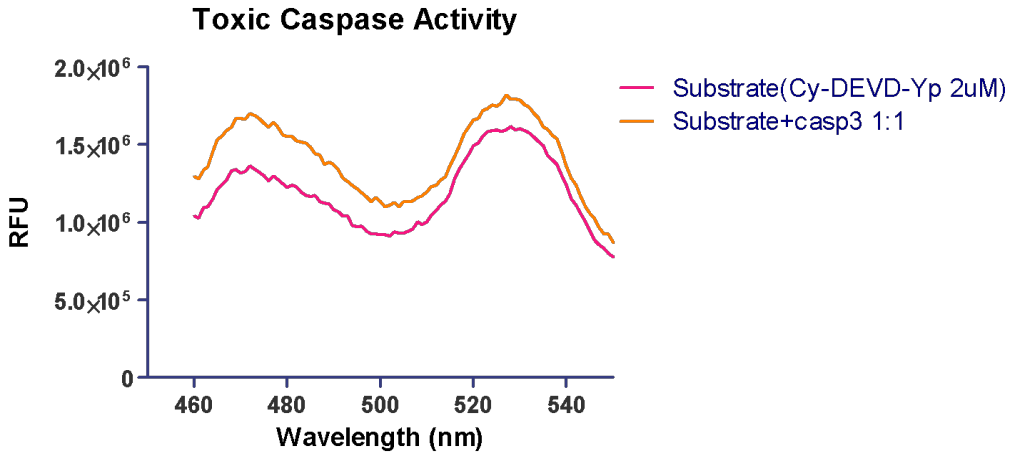

Figure 29. FRET assay to detect Apoptosis. Addition of caspase to the substrate DEVD has no effect. The behavior is as if no enzyme has been added.

Induced overnight at 37˚C

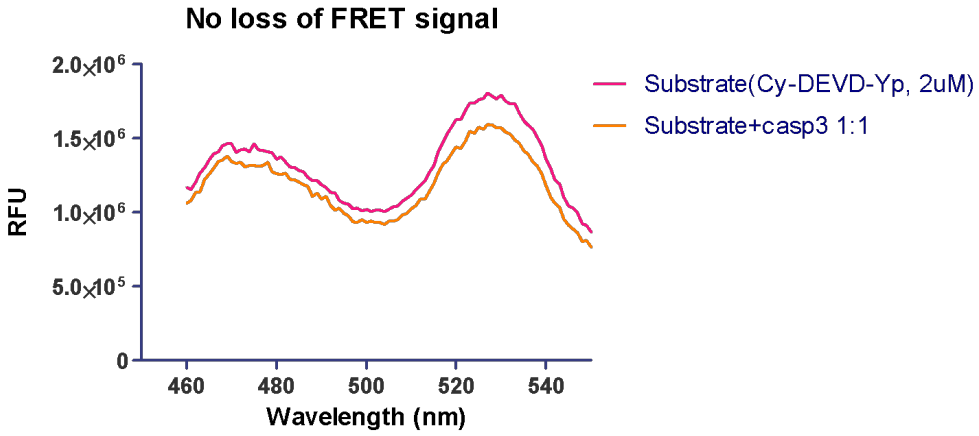

Figure 30. FRET assay to detect Apoptosis when induced overnight at 37˚C. This figure suggests that caspase has not been purified successfully when induction is done overnight at 37°C.

Induced for 2 hours and resuspended with protease inhibitors

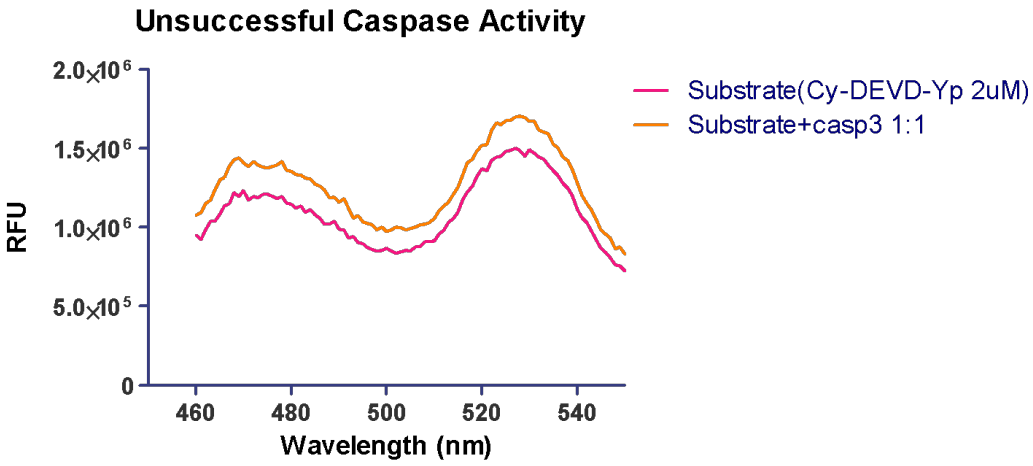

Figure 31. Unsuccessful FRET assay to demonstrate Apoptosis. This figure is yet another instance when caspase addition did not result in Apoptosis

Induced for 1 hour

When procaspase is incubated with substrate containing the peptide DEVD sequence, procaspase is automatically cleaved to caspase that in turn cleaves DEVD resulting in apoptosis.

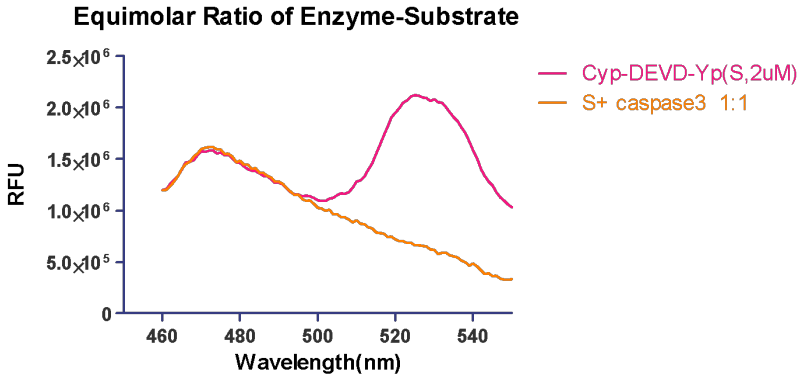

Figure 32. FRET assay demonstrating successful caspase activity. The graph above demonstrates the decrease in signal intensity at 530nm corresponding to the amount of digested substrate. The loss in FRET signal measured at 530nm is almost 4 times the original value in the absence of enzyme.

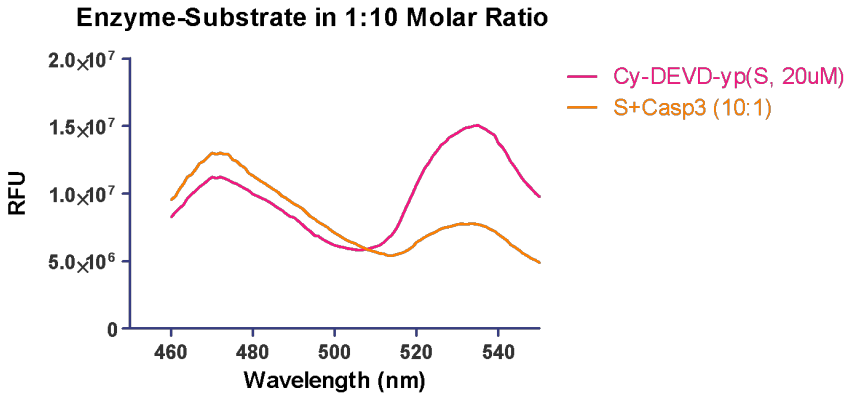

Figure 33. Caspase activity when substrate is ten times more than enzyme. When substrate concentration is increased to ten times the enzyme concentration, it is seen that the signal at 530nm is still decreased although not as much when they were in equimolar ratio.

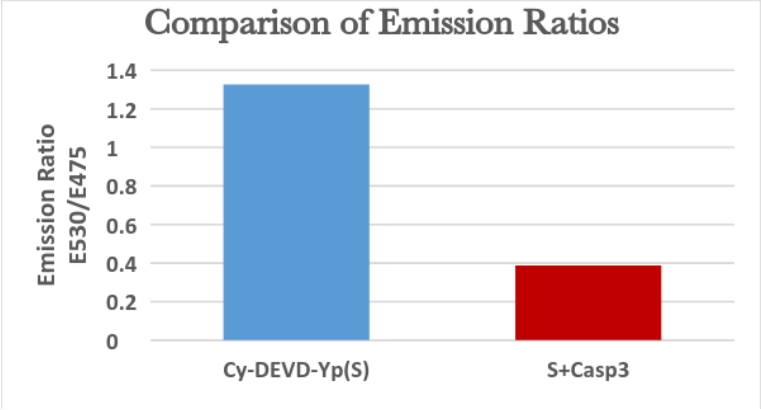

Figure 34. Emission ratio comparison. Bar graph shows a significant decrease in emission ratio as emission of acceptor decreases and donor increases when caspase-3 is added to Cypet-DEVD-Ypet. The emission ratio is a sensitive measurement of enzyme cleavage activity.

Autophagy Peptide FRET Assay

CyPet-LC3B-Gate16-Ypet (2uM) was mixed with Atg4A in a 1:1 molar ratio along with a suitable buffer (50mM Tris–HCl Ph 8, 150mM NaCl, 1mM DTT) to a total volume of 60ul and incubated for 60 min at 37°C. To serve as control, the substrate CyPet-LC3B-Gate16-Ypet was mixed with the same buffer to a total volume of 60ul and incubated at the same temperature for the same time. Fluorescence signals were determined by the fluorescent plate reader, Flexstation II384 (Molecular Devices, Sunnyvale, CA). Emission intensities were collected at two wavelengths: 475 and 530 nm at an excitation wavelength of 414 nm. As can be seen from figure 36, Atg4A is unable to cleave peptide sequences of LC3B and Gate-16. There is no loss of FRET signal on addition of Atg4A. To overcome this problem, I set to remake the autophagy substrate by using full length Gate-16 protein.

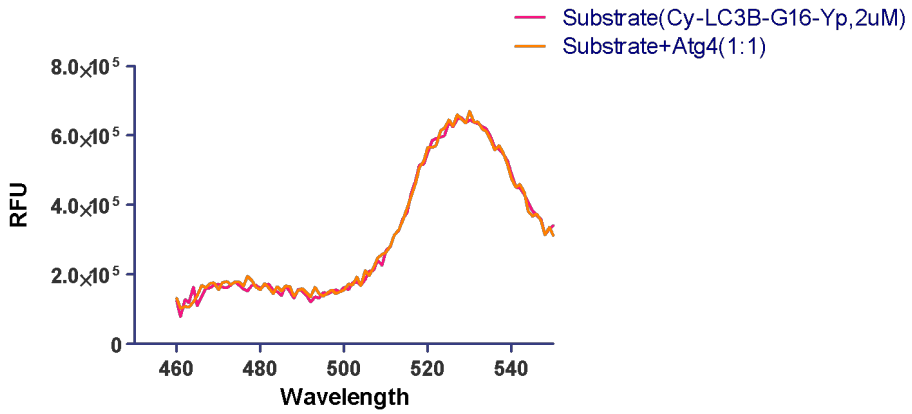

Figure 35. Unsuccessful Autophagy FRET Assay. A peak at 530nm can be seen in the above graph confirming presence of FRET when excited at 414nm. Also seen is the lack of a decrease in FRET when Atg4 is added in equimolar concentration as the substrate.

Autophagy Full Length FRET Assay

CyPet-Gate16-Ypet (2uM) was mixed with Atg4A in a 1:1 molar ratio along with a suitable buffer (50mM Tris–HCl Ph 8, 150mM NaCl, 1mM DTT) to a total volume of 60ul and incubated for 60 min at 37°C. To serve as control, the substrate CyPet-Gate16-Ypet was mixed with the same buffer to a total volume of 60ul and incubated at the same temperature for the same time. The mixture was transferred to a 384 well plate and readings were taken from Flexstation II (Molecular Devices Inc) by providing excitation signals at 414nm. The emission intensity is measured in Relative Fluorescence Units(RFU) and plotted on the y-axis. Wavelength measured in nm is plotted on the x-axis.

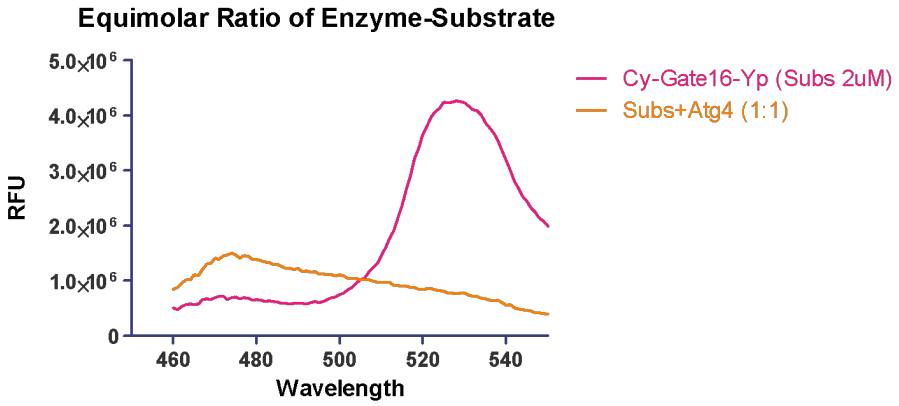

Figure 36. Successful Autophagy FRET Assay. From the graph above we can see the loss in signal intensity corresponding to FRET at 530nm and a corresponding rise in Cypet emission at 475nm. There is more than four times decrease in FRET signal as Atg4A cleaves the substrate Cypet-Gate16-Ypet. This decrease is directly proportional to the concentration of substrate digested.

To take it forward, the concentration of substrate was increased to ten times the concentration of enzyme, to assay efficiency of Atg4A. FRET signal reduced to three times the value it was in the absence of enzyme.

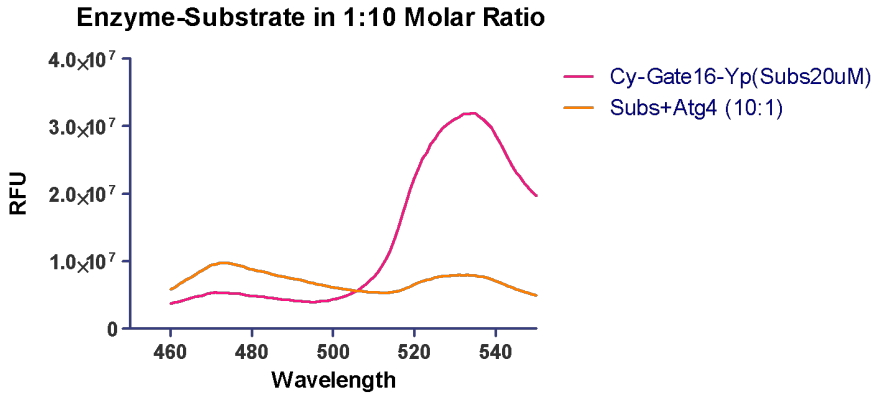

Figure 37. Atg4A activity when substrate is ten times more than enzyme. From the graph above we can see the loss in signal intensity corresponding to FRET at 530nm and a corresponding rise in Cypet emission at 475nm

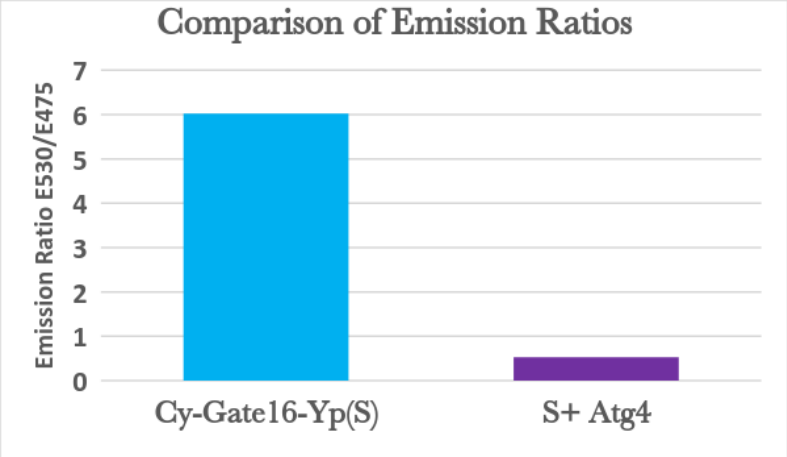

Figure 38. Emission ratio comparison. Bar graph shows a significant decrease in emission ratio as emission of acceptor decreases and donor increases when Atg4 is added to Cypet-Gate16-Ypet.

Discussion

Here, we have report the development of a highly sensitive FRET-based Biosensor to detect Apoptosis and Autophagy pathways. The efficiency of the Biosensor lies in the use of the highly optimised FRET pair Cypet-Ypet and a robust construct design that can detect the execution phase of Apoptosis and Autophagy in the most efficient manner. Our results reveal that pro-caspase-3 can undergo autoproteolysis during the process of purification to yield caspase-3 and that can be toxic to the cells. This can be avoided by controlling the expression of procaspase-3 so that it stays in its inactive form and undergoes proteolysis only when required. This can be done by ensuring that protein expression is not induced for more than three hours. The results also show that Atg4A is unable to cleave peptide sequences of Gate-16 although the cleavage site is exposed for the enzyme. This implies the existence of a dynamics between Atg4A and Gate-16 such that every domain of the Gate-16 protein counts.

CHAPTER 3

MEASUREMENT OF ENZYME KINETICS OF ATG4 USING QUANTITATIVE FRET METHOD

Abstract

Cell Death pathways usually involve proteases that cleave a multitude of proteins thus serving as effectors and executing the death process. One such protease is Atg4A which plays an important role in the ubiquitin conjugation system of the autophagy pathway.

Atg4A is a cysteine protease that cleaves the Atg8 homologue, namely Gate-16 at the carboxyl terminus to expose the glycine residue that is necessary for subsequent reactions. Understanding the dynamics of Atg4A is key to gain an in-depth knowledge of the autophagy pathway. The catalytic efficiency or specificity of an enzyme is best characterized by the ratio of the kinetic constants, k_{cat}/k_m. Previous attempts to establish the kinetic parameters were attempted by using the classic SDS-PAGE gel method. However, the polyacrylamide-gel-based techniques are laborious and technically demanding and do not readily lend themselves to detailed quantitative analysis. The k_{cat}/k_m values obtained using the enzyme tagged with GST tag is also many orders of magnitude lower than the natural substrate[45].

FRET-based protease assays have been used to study Atg4A kinetics using the FRET pair of cyan fluorescent protein (CFP) and yellow fluorescent protein (YFP) in the literature. The ratio of acceptor emission to donor emission was used as the quantitative parameter for FRET signal monitor for protease activity determination. However, this method ignored

signal cross-contaminations at the acceptor and donor emission wavelengths by acceptor and donor self-fluorescence and thus was not accurate[46].

We developed a highly sensitive and quantitative FRET-based protease assay for determining the kinetic parameters of Gate16 digestion by Atg4A. An engineered FRET pair CyPet and YPet was used to generate the CyPet-Gate16-YPet substrate. We differentiated and quantified absolute fluorescence signals contributed by the donor and acceptor and FRET at the acceptor and emission wavelengths, respectively. The value of k_{cat}/k_m of Atg4A toward Gate16 was obtained as 5.2 $x10^4$ $M^{-1}s^{-1}$ which agrees with general enzymatic kinetic parameters. Therefore, this methodology is valid and can be used as a general approach to characterize other proteases as well.

Introduction

Enzymes are organic catalysts that alter the rate of chemical reaction. They also possess remarkable specificity in that they generally catalyze the conversion of only one type (or at most a range of similar types) of substrate molecule into product molecules. There are two theories that describe the binding of enzymes: 1) Lock and Key Theory and 2) Induced Fit Theory.

1) Lock and Key Theory: The shape of the enzyme's active site is complementary to that of its substrate

2) Induced Fit Theory: The active site has a flexibility of shape, thus when an appropriate substrate is in contact with the enzyme's active site, the shape of the active site would change to fit with the substrate. This is depicted schematically in (fig 39).

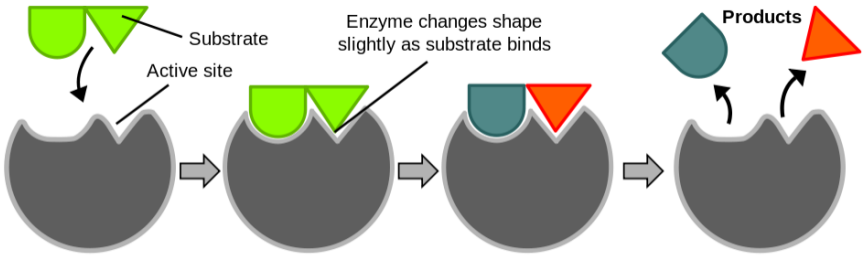

Figure 39. Diagram illustrates how the enzyme binds to the substrate by the induced fit theory

An adhoc function used to describe enzyme kinetics is the Michealis-Menten function which is of the form :

$$v_p = \frac{V_{max}\ S}{K_m + S} \qquad \text{[Eq. 1]}$$

where v_p is the velocity with which a metabolic substrate S is converted into a product P with the help of an enzyme E. The function has two parameters. Vmax is the maximum speed v_p can reach, while K_M is the substrate concentration for which v_p runs with half the maximum speed. The enzyme substrate dynamics can be pictorially represented as shown in (fig 40).

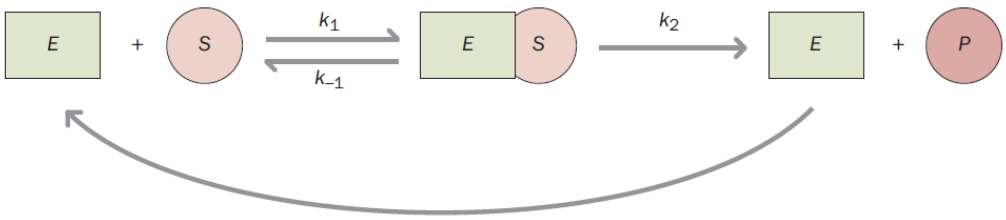

Figure 40. Enzyme-Substrate dynamics. Substrate S and enzyme E form a complex ES, which may revert to S and E or break down to yield product P while releasing the enzyme. k1 is the rate constant of the forward reaction, k-1 is the rate constant of the reverse reaction. k2 is the rate at which the enzyme-substrate complex breaks down into product and free enzyme[48,49,50,51]

The values of the enzyme's catalytic efficiency k_{cat}/k_m is used to compare the utilization of different substrates for an enzyme. It also indicates the efficiency with which the enzyme catalyzes a reaction both in the forward and reverse directions. The accuracy of proteases kinetic parameters is not only important for understanding protease activity in normal physiological processes but also critical for estimating inhibitor potency and efficacy for drug discovery and development. Several methods are commonly used to determine k_{cat}/k_m, such as the enzymatic digestion in solution, followed by the polyacrylamide gel based western blot method, radioactive-labeled substrate, dialysis of digested substrate, fluorescent compound-labeled peptide substrate, and fluorescent protein-labeled substrate[44]. Previous methods to characterize Atg4A enzyme efficiency parameters have been attempted on substrate Gate-16-GST by using SDS-PAGE technique along with Coomassie Blue staining. The amount of substrates as well as cleaved products were quantified by densitometry and the use of GST standard curve[45]. The k_{cat}/k_m obtained using this method was $1 *10^4$ mol^{-1} litre s^{-1}. Assessment of Atg4 activity has been mainly based on an SDS-PAGE-based assay which can be cumbersome and highly variable with a relatively low detection sensitivity. These methods would be only suitable for in vitro analysis and cannot be formatted for high-throughput analysis[46]. FRET based kinetic analysis has also been studied on full length Gate-16 using the parental CFP-YFP. The value of k_{cat}/k_m obtained using this method was 1,310 mol^{-1} litre s^{-1} which was even lower than that obtained when GATE-16-GST was used. In this chapter, I will describe the development of a highly sensitive FRET based protease assay to study the protease activity of Atg4A. An engineered FRET pair, CyPet and YPet, with significantly improved FRET

efficiency and fluorescence quantum yield[43], was used to generate the Cypet-Gate16-Ypet substrate. I have adopted the novel methodology of determination of kinetic parameters of enzyme from Yan Liu's work[45]. This method includes the application of quantitative FRET analysis along with the considerations of the self-fluorescence of donor and acceptor to Gate-16 digestion by Atg4A. The absolute fluorescent signals were converted into protein concentrations using the real-time detection method. The methodology can be extended to study other proteases as well. In addition, error propagation and analysis has been done using both Graphpad and R statistics (code supplied by Dr Jun Li, UCR Statistics Dept)

Experimental

Plasmid Constructs

The construct encoding CyPet-Gate16-YPet was cloned into the pET28 (b) vector (Merck KGaA, Germany), engineered with an N-terminal 6xHistidine tag as described previously.

Construct to determine donor self-fluoresence α

The open reading frame of CyPet and Gate-16 was amplified using forward primer containing the portion of Pet28b vector sequence 3' to Nhe-1 site and reverse primer containing the reverse complement of the cleaved portion of Gate16 as well as the portion of Pet28b vector 3' to Xho1 site. Previously developed Cypet-Gate16-Ypet was used as template. The construct was designed to have three restriction enzyme sites Xho-1, Hind-III, Sal-1 in the same order from the C-terminus of Cypet to the N-terminus of Gate-16. Pet28b vector was digested at Nhe1 and Xho1 sites using restriction enzyme and standard digestion protocol. The concentration of the PCR fragment, Pet28b(overlap)-Cypet-Xho1-

HindIII-Sal1-Gate16(cleaved) along with the digested vector fragment was measured using nanodrop. The fragments were incubated with 10ul NEB Master Mix in a 1:1 ratio for 1 hour at 50°C. The mixture was then transformed into TOP10 Escherichia cells and the colonies screened to get the positive clone. The construct Cypet-Xho1-Hind3-Sal1-Gate16(cleaved) was obtained after sequencing results were confirmed.

Protein Expression and Purification

Escherichia coli cells of strain BL21 (DE3) were transformed with pET28 vectors encoding Atg4A, CyPet-Xho1-HindIII-Sal1-Gate16-Bamh1-Nhe1-Ecor1-YPet and CyPet-Xho1-HindIII-Sal1-Gate16 (cleaved) and protein purification and expression was carried out as described previously.

Fluorescence Spectrum Analysis of FRET

When substrate Cypet-Gate16-Ypet is excited at 414nm, the emission at 475nm was from the emission of unquenched CyPet (FL_{DD}). The emission intensity at 530 nm (FL_{DA}) consists of three components: the direct emission of unquenched CyPet (FL_{DD}), the direct emission of YPet (FL_{AA}) and the emission of YPet excited by energy transferred from CyPet (Em_{FRET}). Excited at 475 nm, an emission peak at 530nm (FL_{AA}) was observed from the direct excitation of YPet but not CyPet. The direct emission of donor, CyPet, at 530nm was proportional to its emission at 475nm when excited at 414 nm with a ratio factor of α, while the direct emission of acceptor, YPet, at 530 nm was proportional to its emission at 530nm when excited at 475nm with a ratio factor of β. Therefore, the FRET emission of YPet (Em_{FRET}) can be determined by:

$$\text{EmFRET} = FL_{DA} - \alpha\, FL_{DD} - \beta\, FL_{AA} \qquad \text{[Eq 2]}$$

The concept of the FRET signal breakup is as shown in figure 41:

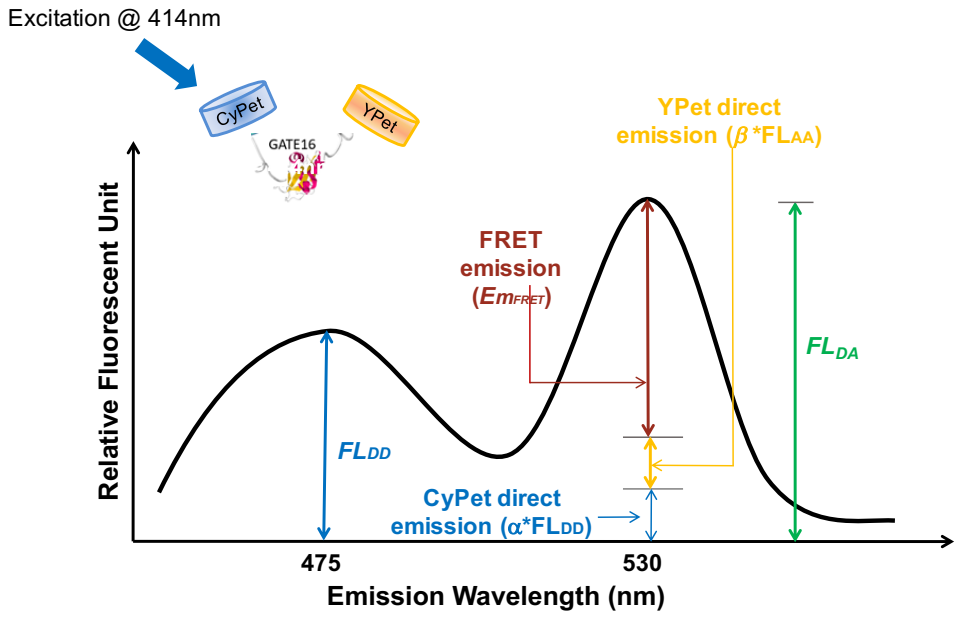

Figure 41. Spectrum analysis of detected emission at 530 nm. Dissection of emission spectra from the engineered protein CyPet–Gate-16–YPet when excited at 414 nm. FL_{DD} is CyPet fluorescence at 475 nm when excited at 414 nm, Em_{FRET} is FRET-induced YPet emission at 530 nm when excited at 414 nm, and FL_{AA} is direct YPet emission at 530 nm when excited at 475 nm.

Direct Emission Characterization by Correlation Coefficiency

To overcome the issue of signal bleed through, direct emission of donor and acceptor in the FRET channel was figured out and subtracted to get the actual FRET signal as shown in (fig 42).

A)

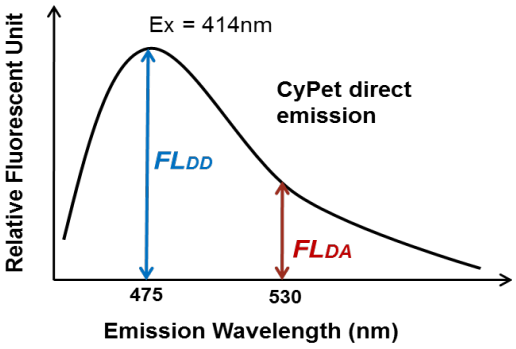

$$\alpha = \frac{FL_{DA}}{FL_{DD}}$$

B)

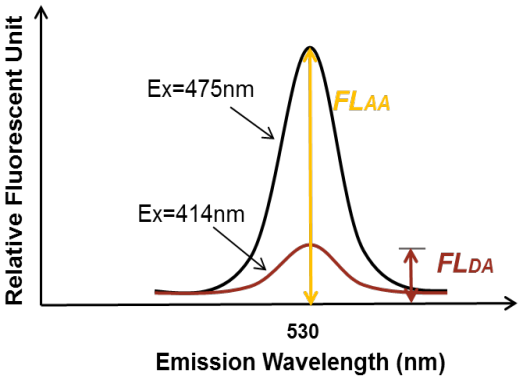

$$\beta = \frac{FL_{DA}}{FL_{AA}}$$

Figure 42. Spectrum analysis of FRET signal. (**A**). Spectrum analysis of direct emission of donor (CyPet). FL_{DD} is the fluorescent emission of CyPet-Gate16 at 475 nm when excited at 414 nm; FL_{DA} is the fluorescent emission of CyPet-Gate16 at 530 nm when excited at 414 nm. (**B**). Spectrum analysis of direct emission of acceptor (YPet). FL_{AA} is the fluorescent emission of YPet at 530 nm when excited at 475 nm; FL_{DA} is the fluorescent emission of YPet at 530 nm when excited at 414 nm.

Standard Curve Analysis

CyPet-Gate-16-YPet was incubated at 37°C in a suitable buffer (50mM Tris–HCl Ph 8, 150mM NaCl, 1mM DTT) to a total volume of 80 µl and added to each well of a 384-well plate. The emission signals at 475 nm were collected after excitation at 414 nm. The concentration was varied from 0.1 to 1 µM. CyPet-Gate16(cleaved) and YPet were also

incubated at 37°C in the same buffer to a total volume of 80 µl with 1:1 molar ratio and added to each well of a 384-well plate. The emission signals at 475 nm were collected after excitation at 414 nm. The concentration of CyPet-SUMO1 was varied from 0.1 to 1 µM. Slopes value were obtained as 459000 and 713000 respectively, describing the linear relationship between the detected fluorescent signals and the protein concentrations.

A) B)

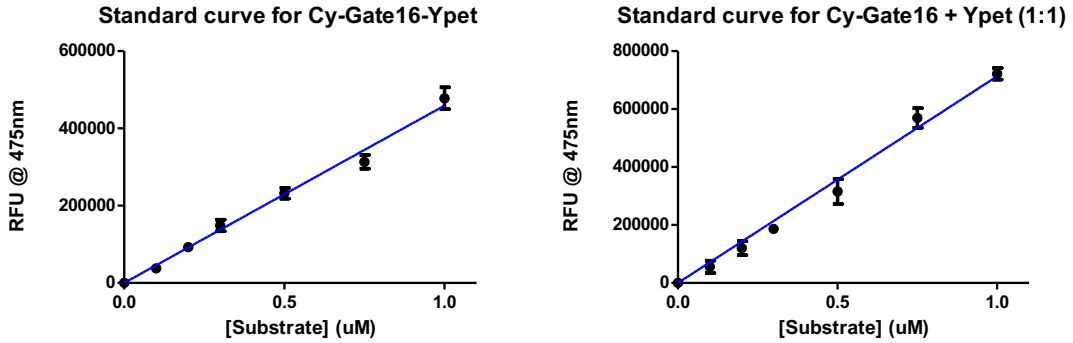

Y = 459000X Y = 713000X

Figure 43. Standard curves of fluorescent signal versus related protein concentration a) Emission of Cypet-Gate16-Ypet at 475nm under excitation at 414nm; b) Emission of CyPet-Gate16 + YPet (1:1) at 475nm under excitation at 414 nm.

Determine Digested Substrate Concentration from the FRET Signal Changes

After digestion by Atg4A, the fluorescent signal at 530 nm decreased, and the fluorescent signal at 475 nm increased because of the disruption of FRET signal after substrate digestion. The remaining fluorescent emission at 530 nm (Em'$_{FRET}$) could still be divided into a similar three components as shown in (fig 45):

$$Em'_{FRET} = FL'_{DA} - \alpha\, FL'_{DD} - \beta\, FL'_{AA} \qquad \text{[Eq. 3]}$$

where FL'$_{DA}$ is the remaining FRET-induced acceptor emission, FL'$_{DD}$ is the fluorescent emission of CyPet, which consists of two parts: the undigested CyPet-Gate16-YPet and the

digested CyPet-Gate16, and FL'$_{AA}$ is the fluorescent emission of YPet, which is constant whether substrate is digested or not.

The amount of digested substrate is correlated with the decrease of absolute FRET signal. Therefore, after treatment with Atg4A, the remaining FRET-induced acceptor's emission (Em'$_{FRET}$) :

$$\frac{C-x}{C} * \mathrm{Em}_{\mathrm{FRET}} = \frac{C-x}{C} * (\mathrm{FL}_{\mathrm{DA}}) - \alpha(\mathrm{FL}_{\mathrm{DD}}) - \beta(\mathrm{FL}_{\mathrm{AA}}) \qquad \text{[Eq. 4]}$$

where C is the concentration of substrate(uM) and x is the concentration of digested substrate(uM).

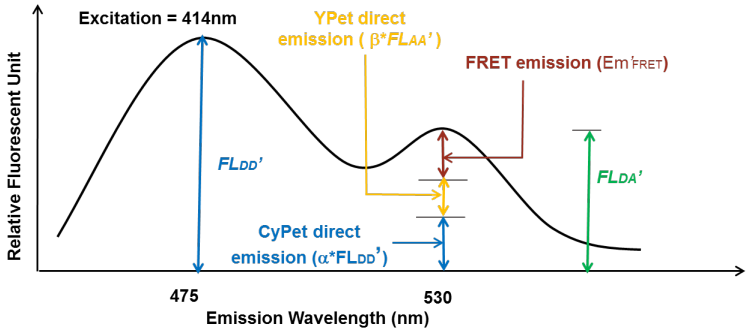

Figure 44. Spectrum analysis of detected emission at 530 nm. Dissection of emission spectra from the engineered protein CyPet–Gate-16–YPet when excited at 414 nm. FL'$_{DD}$ is CyPet fluorescence at 475 nm when excited at 414 nm, Em'$_{FRET}$ is FRET-induced YPet emission at 530 nm when excited at 414 nm, and FL'$_{AA}$ is direct YPet emission at 530 nm when excited at 475 nm.

RESULTS

FRET Assay

To determine the cross-talk ratio of CyPet's self-fluorescence, purified CyPet-Gate16 was incubated in buffer containing 20 mM Tris-HCl, pH 7.4, 50 mM NaCl, and 1 mM DTT to

a total volume of 80 µL at concentrations of 20, 50, 100, 200, 500nM, 750nM and 1000nM and added to each well of a 384-well plate (Greiner, glass bottom).

Fluorescent emissions of CyPet at 475 and 530 nm were detected in a fluorescence multi-well plate reader (Flexstation II384, Molecular Devices, Sunnyvale, CA, USA) when excited at 414 nm to determine the cross-talk ratio α. Three samples were repeated for each concentration. Ypet's self-flourescence determined by cross-talk ratio β was summarized from results obtained previously in the lab. The reason I repeated α calculation and not β was because α showed slight variation depending on the protein that was linked to Cypet maybe because of the structural differences in the protein of interest. But average value of β remained constant at 0.026.

Cypet-SUMO1	Cypet-SUMO2	Cypet-SUMO3	Cypet-Gate16
0.332±0.07	0.278±0.06	0.265±0.05	0.38±0.02

Table 1. α values for different donor proteins obtained previously in the lab. Shown in blue is the α value of Cypet-Gate16 as obtained by me. This value will be considered for future calculations.

Titration Assay

To determine the ratio of enzyme: substrate needed for efficient cleavage, I conducted a titration assay by keeping the substrate concentration constant (1000nM) and varying enzyme concentration from 0.1nM to 1000 nM. The mixture was incubated at 37°C for 1 hour and transferred to 384 well plate. It can be concluded that for my biosensor to detect

autophagy at 37˚C in 1 hour, the enzyme: substrate concentration should be at least 1:20 (fig 45).

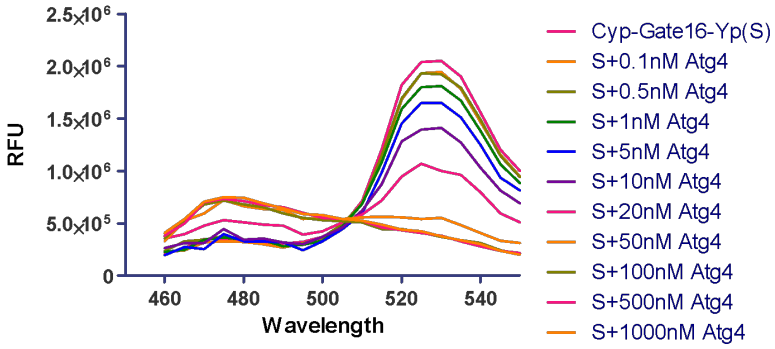

Figure 45. Titration assay. Above spectrum displays the steady decrease in FRET signal shown by a loss in signal intensity at 530nm with increase in enzyme concentration.

Protease Kinetics Assay

FRET-based kinetic assays were conducted by using the kinetic spectrum in a fluorescence multi-well plate reader (Flexstation II$_{384}$, Molecular Devices) that was set to 37˚C. The spectrum setting was as follows:

Excitation Wavelength(nm)	Emission Wavelength (nm)	Cutoff(nm)
414	475	455
414	530	515
475	530	515

Table 2. Wavelength settings in Flexstation II for the kinetic assay.

The substrate CyPet-Gate16-YPet at different concentrations starting from 0.1uM, 0.2uM, 0.3uM, 0.5uM, 0.75uM, 1uM, 2uM, 3uM, 5uM, 10uM and 15uM was incubated in a suitable buffer (50mM Tris HCl Ph 8, 150mM NaCl and 1mM DTT) to a total volume of 80ul at 37°C and transferred to each well of a 384-well plate (Greiner, glass bottom).

Readings were taken every 52 secs for one hour. Atg4A is then added at a concentration of 10nM to the substrate using a multichannel pipette. Same readings were repeated. The data was imported into MS Excel. Background signal was subtracted from the original data which was then processed to get Em_{FRET}, Em'_{FRET} and x (amount of digested substrate). The x values are imported into Graphpad in replicate. Curve fit is performed using Nonlinear regression. The concentration of product formation increases exponentially with time from time t=0 when substrate concentration is 0 to a concentration of S_0 at infinite time per the following formula:

$$[P] = [S]_0 (1 - e^{-kt}) \qquad \text{[Eq. 5]}$$

One phase association model with least squares criteria was used to fit the data. Graphpad Prism provides the mean and standard error values of the key parameters of the model, namely the plateau (the substrate concentration at infinite time) and k (the rate constant). Standard deviation of the parameters is calculated by taking the product of standard error and square root of the no of points analyzed for arriving at the result (Table3).

S (uM)	0.10	0.20	0.30	0.50	0.75	1.00	2.00	3.00	5.00	10.00	15.00
$[S]_0$ (uM)	0.04598	0.1203	0.211	0.3954	0.5896	0.8126	1.475	2.202	3.317	5.128	6.597
k	9.99E-04	8.44E-04	8.30E-04	7.12E-04	7.35E-04	6.88E-04	6.81E-04	5.43E-04	4.54E-04	4.00E-04	4.38E-04
std err ($[S]_0$)	2.59E-03	3.08E-03	3.06E-03	5.17E-03	6.10E-03	8.25E-03	1.70E-02	3.81E-02	8.03E-02	1.59E-01	1.99E-01
std err (k)	1.68E-04	5.71E-05	3.14E-05	2.19E-05	1.82E-05	1.60E-05	1.79E-05	1.86E-05	1.97E-05	2.08E-05	2.31E-05
std dev ($[S]_0$)	3.76E-02	4.46E-02	4.43E-02	7.49E-02	8.84E-02	1.20E-01	2.46E-01	5.52E-01	1.16E+00	2.31E+00	2.88E+00
std dev (k)	2.43E-03	8.27E-04	4.55E-04	3.17E-04	2.64E-04	2.32E-04	2.59E-04	2.69E-04	2.85E-04	3.02E-04	3.35E-04

Table 3. depicts the mean, standard error and standard deviation of $[S_0]$ and k

To determine the reaction velocity of Atg4A, the reaction rate (V) was correlated to the change in the amount of substrate (S):

$$V = -\frac{d[S]}{dt} = \frac{d[P]}{dt} \qquad \text{[Eq. 6]}$$

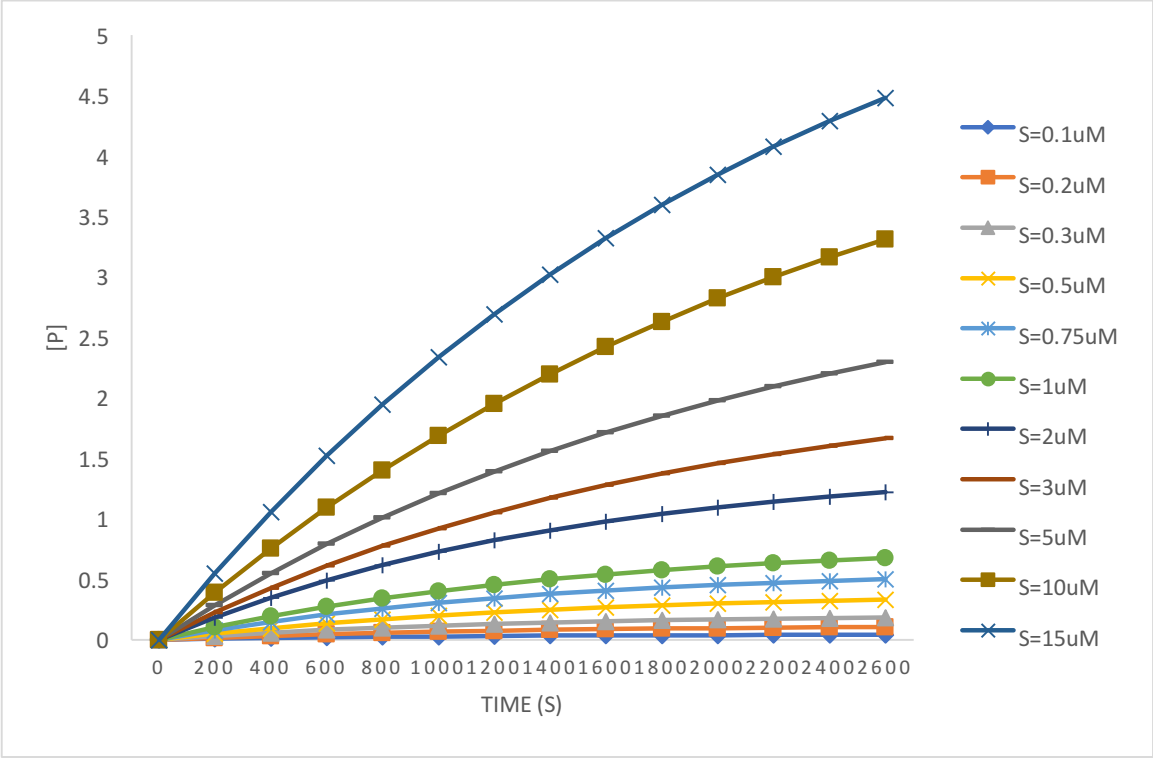

Figure 46. Product time graph showing the digestion of substrate Cypet-Gate16-Ypet by Atg4A

Initial velocity of the reaction is determined by calculating the derivative of product formed at time t=0.

From Eq.5,

$$V_0 = \frac{d[P]}{dt}\Big|_{t=0} = k\,[S_0] \qquad \text{[Eq. 7]}$$

Standard error of V_0 (s_{vo}) is then computed using the formula:

$$s_{v_0}^2 = \{mean(V_0)\}^2 \left[\frac{s_{s_0}^2}{\{mean(s_0)\}^2} + \frac{s_k^2}{\{mean(k)\}^2}\right] \qquad \text{[Eq. 8]}$$

The values obtained are listed below(Table4):

S (uM)	S=0.1	S=0.2	S=0.3	S=0.5	S=0.75	S=1	S=2	S=3	S=5	S=10	S=15
Vo(uM/s)	4.59E-05	1.02E-04	1.75E-04	2.82E-04	4.33E-04	5.59E-04	1.00E-03	1.20E-03	1.51E-03	2.05E-03	2.89E-03
Std error (Vo)	8.13E-06	7.34E-06	7.10E-06	9.40E-06	1.17E-05	1.42E-05	2.88E-05	4.58E-05	7.48E-05	1.24E-04	1.76E-04

Table 4. The initial velocity values obtained along with the Standard error

Michealis -Menten Model

The mean and standard error of Vo is plotted against the substrate concentration in GraphPad Prism V software to fit the Michaelis–Menten equation.

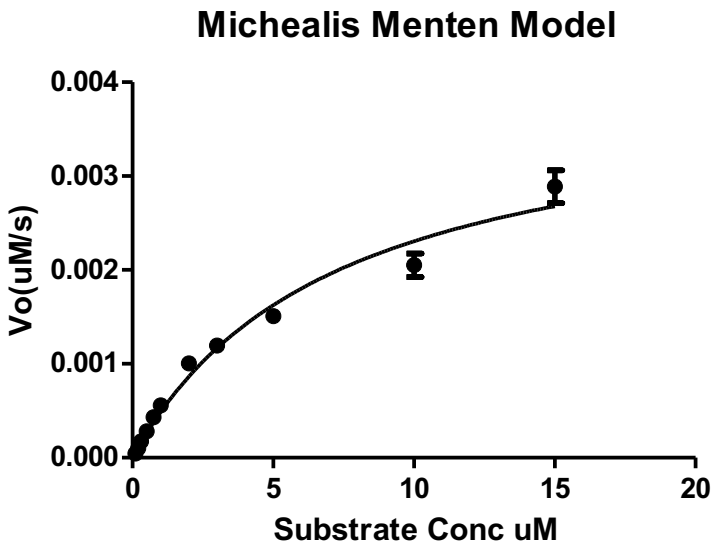

Figure 47. Michaelis-Menten plots of Gate16 digestions by Atg4A

The value of kcat/Km is calculated using the below formula:

$$\frac{k_{cat}}{K_m} = \frac{V_{max}}{K_m}\ x\ 10^8\ \text{mol}^{-1}\text{L s}^{-1} \qquad \text{[Eq. 9]}$$

The standard error of (kcat/Km) is calculated using the following equation:

$$s^2_{kcat/Km} = \{mean(\frac{k_{cat}}{K_M}\}^2\ [\frac{s^2_{kcat}}{\{mean(k_{cat})\}^2} + \frac{s^2_{Km}}{\{mean(Km)\}^2}] \qquad \text{[Eq. 10]}$$

95% confidence intervals were found using Microsoft excel.

The derived values of Vmax, km, k_{cat} and k_{cat}/k_m ratio are listed in the Table 5.

Vmax(mean)	3.96E-03	**Km(mean)**	7.187	**kcat/Km(mean)**	5.51E+04
Vmax(Std error)	3.77E-04	**Km(Std error)**	1.416	**kcat/Km(Std error)**	1.21E+04
				95% CI	6.32E+04
Vmax in uM/s	Km in uM	kcat/Km in $M^{-1}LS^{-1}$			4.70E+04

Table 5. The kinetic parameters that demonstrate the enzyme efficiency of Atg4A

Error analysis was also done using the bootstrap method in R (code provided by Dr Jun Li). The values of kcat/Km and 95% confidence intervals were as follows:

kcat/Km(mean)	5.52E+04
	5.81E+04
95% CI	5.23E+04

Table 6. The kinetic parameters obtained using bootstrap method

Discussion

Here, we have reported the development of a highly sensitive and quantitative FRET-based protease assay for determination of the kinetic parameters of Atg4A in digestion of Gate16. The robust approach used revealed a kcat/Km of 5.5 $*10^4$ mol^{-1} L s^{-1}. In this approach, the absolute FRET signal is correlated to the digested substrate and was continuously determined during the digestions of CyPet-Gate16-YPet substrate by Atg4A. The experimental procedure used here obtains kinetic parameters by deriving the quantitative contributions of absolute fluorescence signals from donor, acceptor, and real FRET at the acceptor's emission wavelength. This quantitative FRET analysis can differentiate the quantitative contributions of each component, whereas traditional ratiometric measurement of FRET cannot. Traditional ratiometric measurements of FRET do not consider the direct emissions and simply convert all of the signal change to disrupted energy transfer. This

results in an overestimation of kinetic parameters from the Michaelis–Menten equation because of an overestimation of FRET emission signal (containing donor and acceptor direct emission) and an overestimation of FRET donor emission (increases with digested substrate)[44,45,46,47].

Gate-16's digestion by Atg4A has been studied by other methods, such as protein gel-based methods used on substrate such as Gate16-GST (Gate16 tagged with GST) and a ratiometric-based FRET assay that used FRET-Gate16 (Gate16 fused between CFP AND YFP) as a substrate. The former established a k_{cat}/k_m value of 12,800 $mol^{-1}S^{-1}$ while a value of 1,310 $mol^{-1}S^{-1}$ was obtained from the latter. Both the techniques used different methods to analyze enzyme efficiency parameters as well as different configuration of substrates. This showed that Atg4A has high specificity towards substrate including the configuration of substrates. The catalytic efficiency of Gate16's digestion by Atg4A was considered as the highest among all of the Gate16-Atg4A digestions. Except the two pre-determined "cross-talk" ratios of donor and acceptor that should be universal for a specific substrate, all the measurements are carried out from one reaction sample. This approach will significantly shorten experimental procedure and also reduce experimental variations because of minimum experimental steps. This methodology can be applied for any FRET pairs and protease in general.

Determination of standard error and 95% confidence intervals of the enzyme efficiency parameters has been done using graphpad as well as bootstrap technique in R. Although kcat/km values obtained were similar using both methods, the confidence intervals have better range using the statistical bootstrap method.

MTT Assays

Background: To take the in vitro reactions to the next level, we decided to transfect mammalian cell lines with the Biosensor, establish stable cell lines and then treat the cell lines with suitable drugs to detect whether the cells died of Apoptosis or Autophagy.

Aim: was to test if sumoylation inhibitors developed by our lab is more potent than commercial drugs in killing cancer cells

Method: We carried out the MTT Colorimetric Cell Proliferation Assay to establish the % of live cells after treatment with drugs. Briefly, H460 large cell lung cancer cell line, H358 non-small cell carcinoma of the lung and Panc-1 human pancreas cell lines were cultured till they were 90-100% confluent. A small volume of the cell suspension was used to count the number of cells in a hemocytometer. A suspension of 5000 cells was made and then seeded in each well of a 96 well plate in triplicate to a total volume of 99ul in 30*3 wells and incubated for 24 hours. Only RPMI media was added to 3 wells for a total volume of 100ul. This served as a control. 3 wells were chosen as blank. The cells were checked under the microscope to ensure good health and inhibitor was added at a working concentration of 10uM to each of the 90 wells. The plate was again placed in the incubator for 24 hours. After changing the media, 20ul of MTS reagent was added to all the wells except the blank and incubated for 1-4 hours. Absorbance at 490nm was measured using the Victor Plate Reader. The absorbance was directly related to the number of live cells in the culture. The same procedure was repeated on H358 and Panc-1 cell lines. The procedure is schematically depicted as shown below:

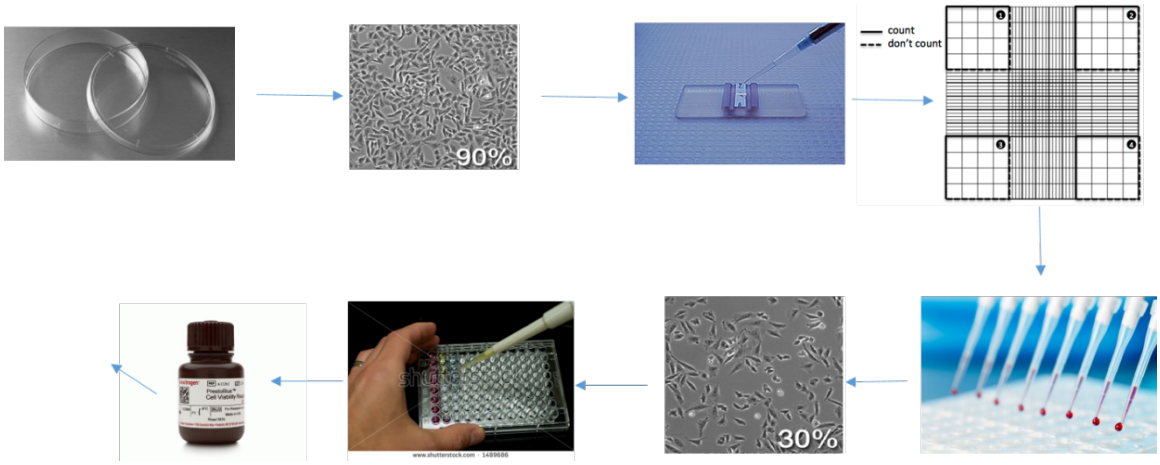

Figure 48. Pictorial representation of the procedure of MTS assay

Results

H358 had a slower growth rate than H460 and Panc-1. For H358, Inhibitors were added 48 hours after cells were seeded as they needed the extra 24 hours to reach the same level of confluency as H460 and Panc-1 cell line. The cells were treated with inhibitor and absorbance was measured after two time periods, 48 hours and 72 hours. Since readings were done in triplicate, mean and SD was computed and error bars were determined. % of cells that were alive was determined by taking the percent ratio of average absorbance of each of the reading and the average control. The results show that sumoylation inhibitors were more effective than other commercial drugs in inhibiting all the cancer cell lines- H460, H358 and Panc-1 (fig 49, 50, 51). These inhibitors could be used to treat cancer cell lines after they were transfected with the Apoptosis and Autophagy Biosensor.

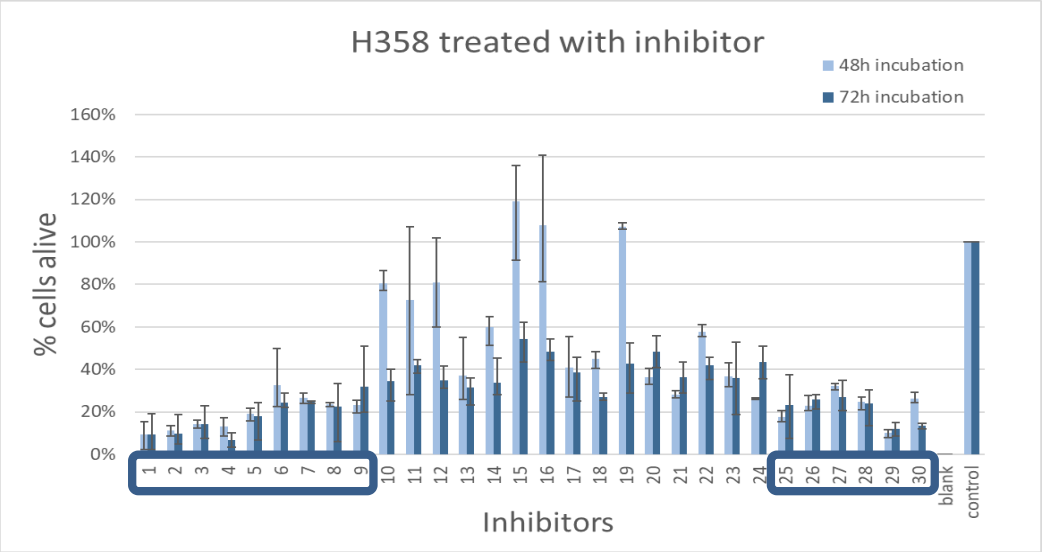

Figure 49. Percentage of cells alive after treatment with inhibitors 1-30. It can be seen from the above graphs that inhibitors 1-9, 25-30 are highly effective at killing the H358 cells. Less than 20% cells are alive after treatment with these inhibitors for 48 hours. After 72 hours of incubation with any inhibitors, not more than 60% of H358 cells are alive. Inhibitors 1-9 are sumoylation inhibitors developed by our lab and inhibitors 10-30 are other commercial drugs.

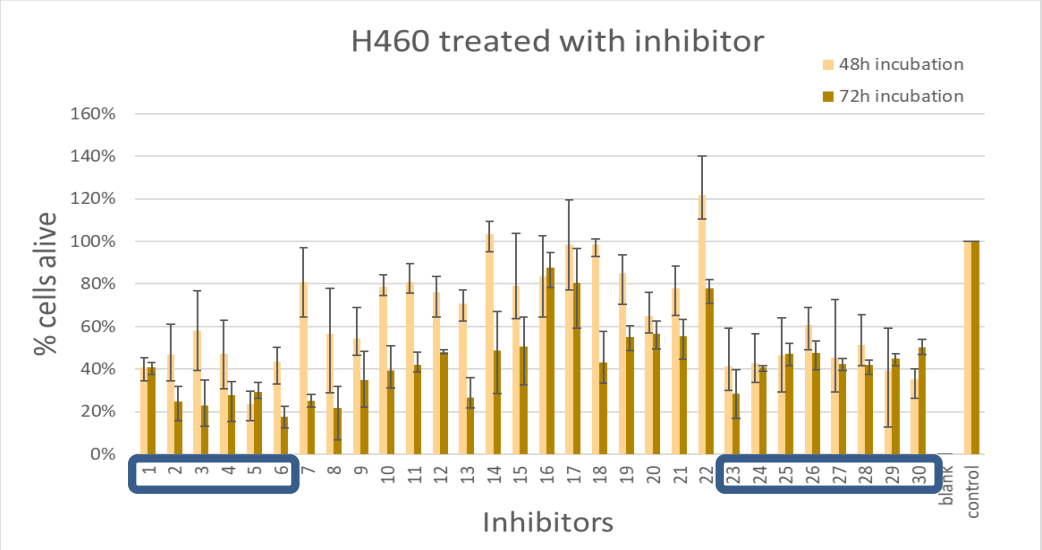

Figure 50. Percentage of H460 cells alive after treatment with inhibitors 1-30. From the above graph it can be concluded that after 48 hours of incubation, Inhibitors 1-6 and 23-30 are most effective at killing cells. For the same incubation period and same concentration, it can be seen that inhibitors are more effective at killing H358 when compared to H460.

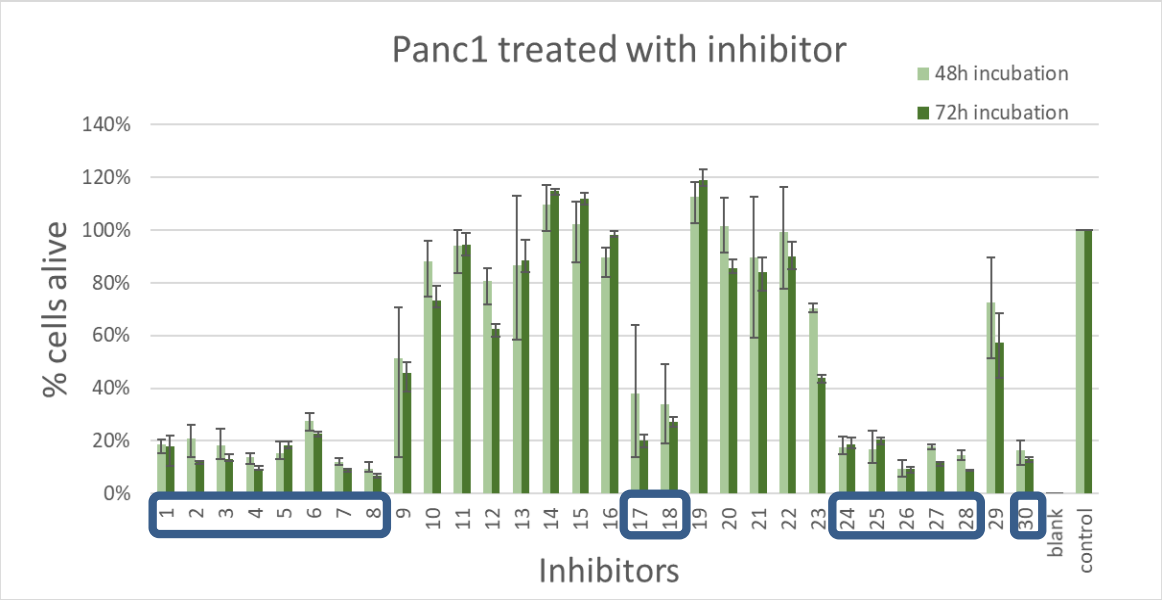

Figure 51. shows the percentage of cells alive after treatment with inhibitors 1-30. It can be seen from the above graphs that inhibitors 1-8, 17-18, 24-28 and 30 are highly effective than the others in inhibiting cancer cells.

Conclusions

In summary, the results of my work show that the biosensors, Cypet-DEVD-Ypet and Cypet-Gate16-Ypet are highly effective in detecting Apoptosis and Autophagy in an in vitro system. These sensors are important as they can also be used to differentiate between Apoptosis and Autophagy. For instance, if I have multiple cell lines treated with the same drug causing cell death, I could potentially transfect the sensors in these cell lines, it would then be feasible to correlate the action of the drug and cell death pathway induced for the cell line in question. For the future work in my lab, these sensors are being transfected in H460 lung cancer cell line to detect cell death caused by action of sumoylation inhibitors. Additionally, the results of Atg4 enzyme kinetics reveals the biochemistry of the enzyme by providing quantitative data in terms of the enzyme efficiency parameters. From the

kinetic studies it can be concluded that Atg4A is unable to cleave peptide sequence of GATE16 as efficiently as opposed to the full length protein. This implies the existence of dynamics between Atg4A and Gate16 that needs further investigation. The value of k_{cat}/k_m obtained through this method is higher than the values obtained previously in literature. This implies that the quantitative FRET method is a better approach to study enzyme kinetics. This could be because of multiple reasons 1. The FRET based assay requires fewer substrate than a gel based assay because of its high sensitivity, 2. The assay is interference free as signals are directly coupled to enzyme activity without involving any secondary reaction, 3. The use of optimized FRET pair Cypet-Ypet in my reaction as opposed to its parental pair CFP-YFP that is used most commonly results in a 20 fold ratiometric FRET signal change. The use of Cypet-Ypet promises improved sensitivity and dynamic range of detection. These results are significant as many high throughput assays that will be based on the protease require thorough knowledge of their Biology. The search for small molecule drugs that target proteases has been a topic of intensive research throughout academics and industry.

References

1. Kepp, Oliver, et al. "Cell death assays for drug discovery." *Nature reviews Drug discovery* 10.3 (2011): 221-237.

2. Kroemer, G., et al. "Classification of cell death: recommendations of the Nomenclature Committee on Cell Death 2009." *Cell death & differentiation* 16.1 (2009): 3-11.

3. Abou-Ghali, Majdouline, and Johnny Stiban. "Regulation of ceramide channel formation and disassembly: Insights on the initiation of apoptosis." *Saudi journal of biological sciences* 22.6 (2015): 760-772.

4. Favaloro, Bartolo, et al. "Role of apoptosis in disease." *Aging (Albany NY)* 4.5 (2012): 330-349.

5. Vermeulen, Katrien, Dirk R. Van Bockstaele, and Zwi N. Berneman. "Apoptosis: mechanisms and relevance in cancer." *Annals of hematology* 84.10 (2005): 627-639.

6. Edinger, Aimee L., and Craig B. Thompson. "Death by design: apoptosis, necrosis and autophagy." *Current opinion in cell biology* 16.6 (2004): 663-669.

7. Duprez, Linde, et al. "Major cell death pathways at a glance." *Microbes and infection* 11.13 (2009): 1050-1062.

8. https://apoptosis2010.wordpress.com/2010/11/23/why-do-cells-undergo-apoptosis/

9. Ellis, Ronald E., Junying Yuan, and H. Robert Horvitz. "Mechanisms and functions of cell death." *Annual review of cell biology* 7.1 (1991): 663-698.

10. http://www.wisegeek.org/what-is-apoptosis.htm#diagram-of-apoptosis

11. https://www.biooncology.com/pathways/cancer-tumor-targets/bcl-2/bcl-2-family-proteins.html

12. Nicholson, D. W. "Caspase structure, proteolytic substrates, and function during apoptotic cell death." *Cell death and differentiation* 6.11 (1999): 1028-1042.

13. http://www.ebi.ac.uk/interpro/potm/2004_8/Page3.htm

14. https://prosper.erc.monash.edu.au/methodology.html

15. Baehrecke, Eric H. "Autophagy: dual roles in life and death?." *Nature reviews Molecular cell biology* 6.6 (2005): 505-510.

16. Nakatogawa, Hitoshi, et al. "Dynamics and diversity in autophagy mechanisms: lessons from yeast." *Nature reviews Molecular cell biology* 10.7 (2009): 458-467.

17. Mizushima, Noboru, et al. "Autophagy fights disease through cellular self-digestion." *Nature* 451.7182 (2008): 1069-1075.

18. http://www.microbeworld.org/component/jlibrary/?view=article&id=15492

19. Boya, Patricia, Fulvio Reggiori, and Patrice Codogno. "Emerging regulation and functions of autophagy." *Nature cell biology* 15.7 (2013): 713.

20. Moreau, Kevin, Maurizio Renna, and David C. Rubinsztein. "Connections between SNAREs and autophagy." *Trends in biochemical sciences* 38.2 (2013): 57-63.

21. Suzuki, Kuninori, et al. "Hierarchy of Atg proteins in pre- autophagosomal structure organization." *Genes to Cells* 12.2 (2007): 209-218.

22. https://en.wikipedia.org/wiki/MTORC1

23. Mari, Muriel, Sharon A. Tooze, and Fulvio Reggiori. "The puzzling origin of the autophagosomal membrane." *F1000 Biol Rep* 3.25.10 (2011): 3410.

24. https://www.ncbi.nlm.nih.gov/gene?Db=gene&Cmd=DetailsSearch&Term=8678

25. Obara, Keisuke, and Yoshinori Ohsumi. "Atg14: a key player in orchestrating autophagy." *International journal of cell biology* 2011 (2011).

26. Xie, Z. & Klionsky, D. J. Autophagosome formation: core machinery and adaptations. Nature Cell Biol. 9,

27. Nakatogawa, Hitoshi. "Two ubiquitin-like conjugation systems that mediate membrane formation during autophagy." *Essays In Biochemistry* 55 (2013): 39-50.

28. Becker, Esther BE, and Azad Bonni. "Cell cycle regulation of neuronal apoptosis in development and disease." *Progress in neurobiology* 72.1 (2004): 1-25.

29. Lang, Richard A. "Apoptosis in mammalian eye development: lens morphogenesis, vascular regression and immune privilege." *Cell death and differentiation* 4.1 (1997): 12-20.

30. Bennett, Martin R. "Apoptosis in the cardiovascular system." *Heart* 87.5 (2002): 480-487.

31. Kuma, Akiko, et al. "The role of autophagy during the early neonatal starvation period." *Nature* 432.7020 (2004): 1032-1036.

32. Ekiz, Huseyin Atakan, Geylani Can, and Yusuf Baran. "Role of autophagy in the progression and suppression of leukemias." *Critical reviews in oncology/hematology* 81.3 (2012): 275-285.

33. Galluzzi, Lorenzo, et al. "Guidelines for the use and interpretation of assays for monitoring cell death in higher eukaryotes." *Cell Death & Differentiation* 16.8 (2009): 1093-1107.

34. https://en.wikipedia.org/wiki/Immunoperoxidase

35. Garrity, Megan M., et al. "Identifying and quantifying apoptosis: navigating technical pitfalls." *Modern pathology* 16.4 (2003): 389-394.

36. Ibraheem, Andreas, and Robert E. Campbell. "Designs and applications of fluorescent protein-based biosensors." *Current opinion in chemical biology* 14.1 (2010): 30-36.

37. Strianese, Maria, et al. "Fluorescence-based biosensors." *Spectroscopic Methods of Analysis: Methods and Protocols* (2012): 193-216.

38. https://en.wikipedia.org/wiki/F%C3%B6rster_resonance_energy_transfer

39. Swift, S. R., and L. Trinkle-Mulcahy. "Basic principles of FRAP, FLIM and FRET." *Proceedings of the Royal Microscopical Society*. Vol. 39. No. 1. London: Royal Microscopical Society,[1966]-c2004., 2004.

40. Didenko, Vladimir V. "DNA probes using fluorescence resonance energy transfer (FRET): designs and applications." *Biotechniques* 31.5 (2001): 1106.

41. Kochuveedu, Saji Thomas, and Dong Ha Kim. "Surface plasmon resonance mediated photoluminescence properties of nanostructured multicomponent fluorophore systems." *Nanoscale* 6.10 (2014): 4966-4984.

42. Broussard, Joshua A., et al. "Fluorescence resonance energy transfer microscopy as demonstrated by measuring the activation of the serine/threonine kinase Akt." Nature protocols 8.2 (2013): 265-281.

43. Nguyen, A.W. and P.S. Daugherty, Evolutionary optimization of fluorescent proteins for intracellular FRET. Nature Biotechnology, 2005. 23(3): p. 355-360.

44. Jiang, Ling, et al. "Internal calibration förster resonance energy transfer assay: A real-time approach for determining protease kinetics." Sensors 13.4 (2013): 4553-4570.

45. Li, Min, et al. "Kinetics comparisons of mammalian Atg4 homologues indicate selective preferences toward diverse Atg8 substrates." Journal of Biological Chemistry 286.9 (2011): 7327-7338.

46. Li, Min, et al. "A high-throughput FRET-based assay for determination of Atg4 activity." *Autophagy* 8.3 (2012): 401-412.

47. Liu, Yan, et al. "Quantitative Förster resonance energy transfer analysis for kinetic determinations of SUMO-specific protease." *Analytical biochemistry*422.1 (2012): 14-21.

48. Robinson, Peter K. "Enzymes: principles and biotechnological applications." *Essays in biochemistry* 59 (2015): 1-41.

49. https://en.wikibooks.org/wiki/Principles_of_Biochemistry/Enzymes

50. Voit, Eberhard O. *A first course in systems biology*. Garland Science, 2012.

51. Ghobrial, Irene M., Thomas E. Witzig, and Alex A. Adjei. "Targeting apoptosis pathways in cancer therapy." *CA: a cancer journal for clinicians* 55.3 (2005): 178-194.

52. Sgonc R, Gruber J (1998) Apoptosis detection: an overview. Exp Gerontol 33:525–533

53. Sgonc R, Wick G (1994) Methods for the detection of apoptosis. Int Arch Allergy Immunol 105:327–332

54. Martin D, Lenardo M (2001) Morphological, biochemical, and ow cytometric assays of apoptosis. Curr Protoc Mol Biol. doi:10.1002/0471142727.mb1413s49

55. Muppidi J, Porter M, Siegel RM (2004) Measurement of apop- tosis and other forms of cell death. Curr Protoc Immunol. doi:10.1002/0471142735.im0317s59

56. Banfalvi, Gaspar. "Methods to detect apoptotic cell death." *Apoptosis* 22.2 (2017): 306-323.

57. Gu, Chunchuan. "Quantum dots- based fluorescence resonance energy transfer biosensor for monitoring cell apoptosis." *Luminescence* (2017).

58. Tyas, Lorraine, et al. "Rapid caspase- 3 activation during apoptosis revealed using fluorescence-resonance energy transfer." *EMBO reports* 1.3 (2000): 266-270.

59. Lekshmi, Asha, et al. "A quantitative real-time approach for discriminating apoptosis and necrosis." *Cell Death Discovery* 3 (2017): 16101.

60. Klionsky, Daniel J., et al. "Guidelines for the use and interpretation of assays for monitoring autophagy." *Autophagy* 12.1 (2016): 1-222.

61. Barth, Sandra, Danielle Glick, and Kay F. Macleod. "Autophagy: assays and artifacts." *The Journal of pathology* 221.2 (2010): 117-124.

62. https://www.ncbi.nlm.nih.gov/books/NBK92006/

63. Li, M., et al. "Chapter Twelve-Measurement of the Activity of the Atg4 Cysteine Proteases." Methods in Enzymology 587 (2017): 207-225.

64. Bisswanger, Hans. Enzyme kinetics: principles and methods. John Wiley & Sons, 2017.

65. https://chem.libretexts.org/LibreTexts/University_of_California_Davis/UCD_Chem_107B%3A_Physical_Chemistry_for_Life_Scientists/Chapters/2%3A_Chemical_Kinetics/2.10%3A_Fast_Reactions_in_Solution

66. https://chem.libretexts.org/Textbook_Maps/Analytical_Chemistry_Textbook_Maps/Map%3A_Analytical_Chemistry_2.0_(Harvey)/13_Kinetic_Methods/13.2%3A_Chemical_Kinetics

67. Stennicke, Henning R., and Guy S. Salvesen. "Caspases: preparation and characterization." *Methods* 17.4 (1999): 313-319.